

AC

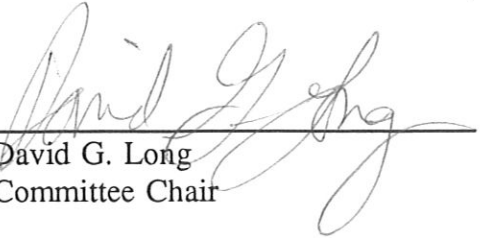
DEVELOPMENT OF A WIRE WAVE GAUGE ARRAY FOR MEASURING WIND-GENERATED WATER WAVES

A Thesis
Submitted to the
Department of Electrical and Computer Engineering
Brigham Young University

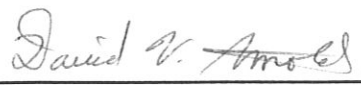
In Partial Fulfillment
of the Requirements for the Degree
Master of Science

by
Charles W. Hedelius
March 1993

This thesis by Charles W. Hedelius is accepted in its present form by the Department of Electrical and Computer Engineering of Brigham Young University as satisfying the thesis requirement for the degree of Master of Science.

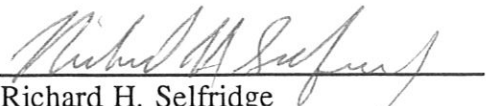


David G. Long
Committee Chair



David V. Arnold
Committee Member

June 11, 1993
Date



Richard H. Selfridge
Graduate Coordinator

ACKNOWLEDGMENTS

I am grateful to Dr. David G. Long and Dr. David V. Arnold for their tireless efforts and great patience in assisting me with many facets pertaining to the successful completion of this research and thesis. In addition, I acknowledge Stephen "Dave" Zimmerman for providing wind data and operation of the weather station during field deployments, and Jacob "Davey" Gunther for assistance on field deployments.

I am greatly indebted to my wife, Jana, for her support during my schooling, and my parents, Dr. & Mrs. R.K. Hedelius, whose generous financial support made my schooling possible.

Mechanical consultation for designing the two-dimensional array was provided by Gene Cook and Vaughn Dearden from BYU college of Engineering and Technology. Plastic storage bins used for field deployments were provided by Charles Cox of BYU Media Services.

CONTENTS

ACKNOWLEDGMENTS	iii
INTRODUCTION	1
THE INSTRUMENT	4
2.1 Theory	4
2.2 Implementation of the Theory	12
2.2.1 Sensor Mechanics	13
2.2.1a One-dimensional "harp" array	13
2.2.1b Two-dimensional array	15
2.2.2 Electronic Hardware	18
2.2.3 Software	19
2.2.4 Sampling Trigger	20
2.3 Instrument Performance	21
2.3.1 Instrument Calibration	22
2.3.2 Accuracy	24
2.3.3 Precision	26
FIELD DEPLOYMENT	32
3.1 Preparation for Deployment	32
3.2 Major Deployments	34
3.3 Deployment Results	36
CONCLUSIONS	46
4.1 Discussion	46
4.2 Future Work	47

LIST OF FIGURES

2.1	Basic electronic circuit for measuring water height	5
2.2	Equivalent circuit for analysis	6
2.3	Output voltage vs. ωRC	9
2.4	Small "Harp" array	14
2.5	Large 2d array	15
2.6	Top view of 2d array including mounting hardware and depiction of broadside and endfire directions	16
2.7	Anchoring of enamel-coated wire on U-bolts for 2d array	17
2.8	Wire mounting hardware for 2d array	17
2.9	Electronic hardware diagram for wire wave gauge	19
2.10	Timing diagram for one array sample	20
2.11	Calibration data vs. linear fit	23
2.12	Typical time series of water wave action	24
2.13	Time series of the average water height on still water	25
2.14	Time series of standard deviation in still water	26
2.15	Time series of standard deviation in agitated water	27
2.16a	Time series of precision for tight wires using two different driving frequency sources	29
2.16b	Time series of accuracy for tight wires using two different driving frequency sources	29
2.17	Time series of precision for loose wires using two different driving frequency sources	30
2.18	Time series of accuracy for loose wires using two different driving frequency sources	31
3.1	Deployment site at Utah Lake	35
3.2	Mechanical generation of waves at Utah Lake	36
3.3	Map of deployment site at Deer Creek Reservoir	37
3.4	Photo of deployment site at Deer Creek Reservoir	38

3.5	Power spectra for wind generated water waves	39
3.6	Comparison of dominant frequency for high wind speeds and low wind speeds	40
3.7	Power spectra for high wind speed	41
3.8	Power spectra for low wind speed	42
3.9	Scatter plot of wind speed vs peak frequency	43
3.10	Comparison of surface roughness for high wind speeds and low wind speeds	44
3.11	Scatter plot of wind speed vs variance	45

CHAPTER 1

INTRODUCTION

The use of electromagnetic waves to detect surface conditions from a remote platform, such as wind and wave patterns over water, has been used successfully for several decades. The major active instruments that provide this function are the scatterometer and the synthetic aperture radar (SAR). Successful space flights involving these instruments include the Seasat mission, and more recently, the ERS-1 mission. These missions have produced an abundance of radar data. However, there remain many questions in the data interpretation because the relationships between radar backscatter and surface conditions are not completely understood. If these relationships were more completely understood, satellites could be deployed that would provide detailed, current information about the surface conditions in remote areas of the world. One application that would produce benefits to the public is knowing the wind over the oceans. Establishing exactly what the wind conditions are in a specific area of the world's oceans would make it possible to route surface vessels around trouble regions, thus reducing damage and risk to life. Another benefit is improved weather forecasting.

In order to improve models that describe the relationship between wind speed and radar backscatter, accurate knowledge of the surface under radar observation must be obtained and compared with radar backscatter data. To provide data which describes surface conditions, an instrument has been developed that measures water waves by digitally recording water wave displacement as a function of time using capacitance wires. This thesis describes the development of this instrument, known as a wire wave gauge array, which has been used to assist scatterometry research at Brigham Young University. The wire wave gauge is deployed with a weather station and a radar. The data from the weather station and wave gauge is merged to provide one data set which contains wave and wind information. This merged data set and the radar data are

compared to develop the mathematical models for obtaining wind speed over the ocean from radar measurements. Therefore, the data from this instrument is the necessary link to develop the essential mathematical models to obtain wind speed from radar data. As mentioned earlier, the development of such models has multiple, practical applications.

The concept of a wave gauge has been used by other researchers in the form of a single wire, or large arrays of resistance or capacitance wires [1-4]. The instrument described herein is unique in that the concept of a capacitance wave gauge has been applied to a small, portable array. The main thrust of this thesis was to develop the instrument and show that it accurately measures wind generated waves. Therefore, analysis of the spatial data, which the array provided is beyond the scope the thesis.

As stated earlier, the overall goal of this research is to provide data to augment scatterometry research. Therefore, the array must be able to detect waves with wavelengths in the range .01 to 10 m, and with amplitudes as small as 1 mm. The smaller wavelengths (.01 m) are primarily the cause of Bragg scattering which is considered to be the most important scattering mechanism. However, larger wavelengths also contribute to scattering at radar frequencies and are, therefore, of interest also.

Chapter 2 is divided into three sections on theory, implementation of the theory and instrument performance. The theory section discusses the concept of the wire capacitor, why it can be used in this application and how it is implemented in an electronic circuit to measure wave displacement. It also discusses how the raw digital voltage measurements are converted to capacitance values, selection of nominal values for the circuit parameters, and the requirements of the computer hardware to operate the system. Implementation of the theory discusses the mechanical structures developed, electronic hardware, and computer software associated with the array. The section on instrument performance further defines resolution, and describes the results of calibration and performance in the laboratory.

Chapter 3 presents preparation for, description of, and major results from various field tests. Preparation discusses the thought and planning that preceded each of the major deployments. The section on major deployments discusses the selection of test sites at Utah Lake and Deer Creek Reservoir. Deployment results discusses the results of

the deployments as they relate to wind-generated water waves. This includes analyses on the power spectrum, dominant frequency, and surface roughness with respect to wind speed. Finally, chapter 4 contains the conclusions of the thesis.

CHAPTER 2

THE INSTRUMENT

To effectively discuss the wire wave gauge array, the discussion will be divided into three sections; 1) theory, 2) implementation of the theory, and 3) instrument performance. The theory section deals with the concept of a wire capacitor, electronic circuitry used to obtain wave data, the theory behind the mean squared error algorithm for computing voltage magnitudes, choosing key electronic parameters, and limits on the computer hardware used to operate the wave gauge. The implementation of the theory section discusses mechanical hardware, and electronic hardware and software. Finally, the section on instrument performance presents details of calibrating the wave data, accuracy and precision of the wave gauge, and the results of various tests to determine the resolution of the instrument.

2.1 Theory

The basis of the wire wave gauge is an array of enamel-coated copper wires. When an enamel-coated wire is immersed into water, there is capacitance between the metal conductor of the wire and the water. The enamel coating on the wire acts as the dielectric of the capacitor. The capacitance, C , of this configuration is given by

$$C = \frac{2\pi\epsilon L}{\ln(\zeta/\xi)} \quad (2.1)$$

where ϵ is the permittivity of the dielectric, L is the length of the wire immersed in the water and ζ and ξ are the radii of the enamel and conductor, respectively [5]. The variation in capacitance for 26 gauge enamel coated copper wire is nominally 8.5 pF/cm (26 gauge wire is the gauge of wire used in one of the arrays). As the water height moves up and down due to wave action, the capacitance varies linearly with the water

height. Thus, by measuring the capacitance of the wire, the height of the water can be inferred. One advantage of using a wire to measure wave action is that its small diameter does not affect the wave propagation significantly; hence, it can provide highly accurate measurements of the wave motion. Furthermore, the wire capacitance can be measured quickly, permitting high frequency sampling of the water wave motion.

A basic electronic circuit for measuring the water height using the wire capacitor is a voltage divider similar to Fig. 2.1. The circuit consists of a known sinusoidal driving source, \tilde{V}_s ; a known resistance, R_f ; a known capacitance, C_f ; and an unknown capacitance, C_w . In addition, there are smaller resistances, R_s , R_w and R_{wtr} . The subscripts stand for source, wire and water respectively. In this circuit, the impedance of R_w and R_{wtr} is very small compared to the impedance of the wire capacitor ($R_w + R_{wtr} \ll 1/j\omega C_w$). Furthermore, R_s is small compared with R_f ($R_s \ll R_f$). Consequently, the resistances R_s , R_w , and R_{wtr} can be omitted for analysis. The unknown capacitance value, C_w , can be calculated from the magnitudes of the source and capacitance voltages \tilde{V}_s and \tilde{V}_c , respectively.

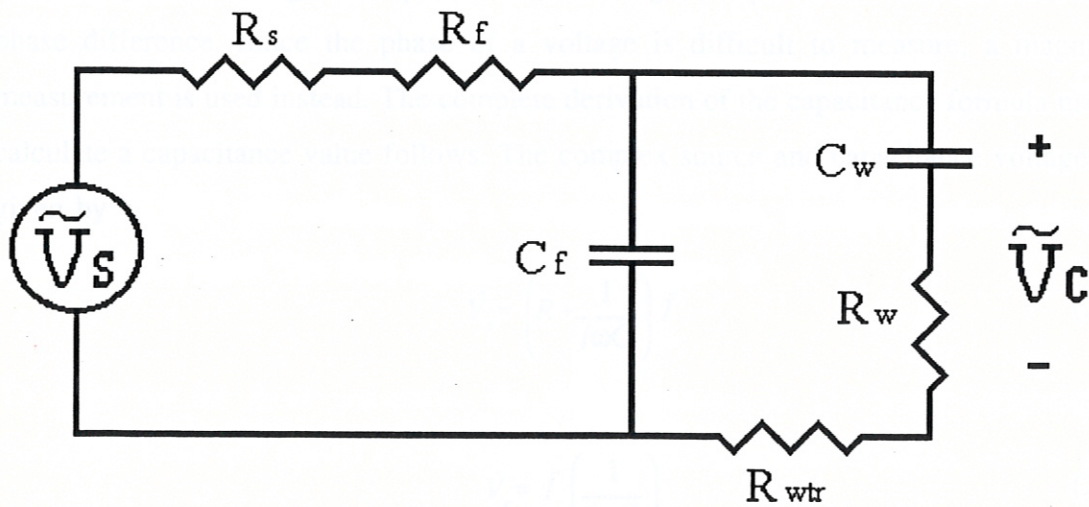


Figure 2.1 Electronic Circuit For Measuring Water Height

The equivalent circuit used for analysis is depicted in Fig 2.2. This circuit depicts only the fixed resistor and the parallel combination of C_f and C_w . This combination

is shown as C_T . Unless explicitly stated otherwise, when capacitor is referenced, it is this parallel combination, C_T .

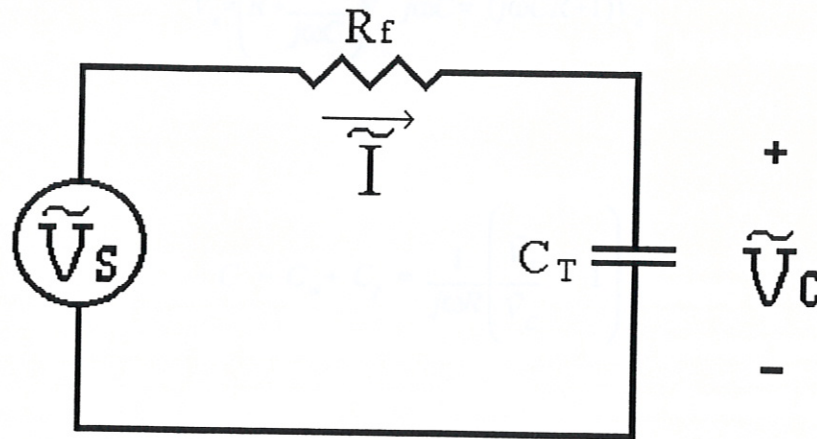


Figure 2.2 Equivalent circuit for analysis.

Because the capacitor introduces a phase lag between the driving voltage and the capacitor voltage, the equation for obtaining the capacitance must account for this phase difference. Since the phase of a voltage is difficult to measure, a magnitude measurement is used instead. The complete derivation of the capacitance formula used to calculate a capacitance value follows. The complex source and capacitance voltages are given by

$$\tilde{V}_s = \left(R + \frac{1}{j\omega C} \right) \tilde{I} \quad (2.2)$$

$$\tilde{V}_c = \tilde{I} \left(\frac{1}{j\omega C} \right) \quad (2.3)$$

Where \tilde{I} is the complex current in the circuit, R ($R \approx R_f$) is the total resistance in the circuit, C is the parallel combination of wire and the fixed capacitor, and ω is $2\pi f$. The

purpose of this fixed capacitor is discussed later in this section. Combining Eqs. (2.2) and (2.3) we get

$$\tilde{V}_s = \left(R + \frac{1}{j\omega C} \right) \tilde{V}_c \quad j\omega C = (j\omega CR + 1) \tilde{V}_c \quad (2.4)$$

where

$$C = C_w + C_f = \frac{1}{j\omega R} \left(\frac{\tilde{V}_s}{\tilde{V}_c} - 1 \right)$$

To account for the phase difference between \tilde{V}_s and \tilde{V}_c , a magnitude formulation is used. This is obtained from Eq. (2.4) by taking the magnitude squared

$$\tilde{V}_s \tilde{V}_s^* = (1 + j\omega RC)(1 - j\omega RC) \tilde{V}_c \tilde{V}_c^* \quad (2.5)$$

which simplifies to

$$|\tilde{V}_s|^2 = (1 + \omega^2 R^2 C^2) |\tilde{V}_c|^2 \quad (2.6)$$

$|\tilde{V}_s|^2$ and $|\tilde{V}_c|^2$ are estimated by a software algorithm, described below, using the digitized wave form. The final equation for capacitance is

$$C = \frac{1}{\omega R} \sqrt{\left| \frac{\tilde{V}_s}{\tilde{V}_c} \right|^2 - 1} \quad (2.7)$$

$|\tilde{V}_s|^2$ and $|\tilde{V}_c|^2$ are computed by fitting the sampled data to a sine wave and computing the minimum mean squared error [6]. The mean squared error is given by

$$\bar{\epsilon}^2 = \sum_{n=0}^{N-1} (f_n - \hat{f}_n)^2 \quad (2.8)$$

where f_n is the n th value of the digitized voltage data and \hat{f}_n is an estimate of the n th value, given by

$$\hat{f}_n = m + \alpha \cos(n\Delta) + \beta \sin(n\Delta) \quad (2.9)$$

where m is the mean value, α and β are fourier series coefficients of the cos and sin terms, and $n\Delta$ is the index (n) multiplied by the discrete time between samples (Δ). The mean value is not used in this research for reasons that will be discussed later. Since the mean squared error is a function of m , α and β , the minimum value is found by taking the derivative of the mean squared error with respect to each of the variables, setting each equation equal to zero and solving for the three unknowns. This is shown mathematically by

$$\begin{aligned} \frac{\partial \bar{\epsilon}^2}{\partial m} &= \sum -2(f_n - m - \alpha \cos(n\Delta) - \beta \sin(n\Delta)) = 0 \\ \frac{\partial \bar{\epsilon}^2}{\partial \alpha} &= \sum -2(f_n - m - \alpha \cos(n\Delta) - \beta \sin(n\Delta)) \cos(n\Delta) = 0 \\ \frac{\partial \bar{\epsilon}^2}{\partial \beta} &= \sum -2(f_n - m - \alpha \cos(n\Delta) - \beta \sin(n\Delta)) \sin(n\Delta) = 0 \end{aligned} \quad (2.10)$$

To solve for the three unknowns, the three equations in (2.10) are separated into individual sums and placed into matrices. The resulting matrix equation, written in the

form $\delta=AX$, is

$$\begin{matrix} \delta \\ \left[\begin{array}{l} \sum f_n \\ \sum f_n \cos(n\Delta) \\ \sum f_n \sin(n\Delta) \end{array} \right] \end{matrix} = \begin{matrix} A \\ \left[\begin{array}{lll} \sum 1 & \sum \cos(n\Delta) & \sum \sin(n\Delta) \\ \sum \cos(n\Delta) & \sum \cos^2(n\Delta) & \sum \sin(n\Delta)\cos(n\Delta) \\ \sum \sin(n\Delta) & \sum \cos(n\Delta)\sin(n\Delta) & \sum \sin^2(n\Delta) \end{array} \right] \end{matrix} \begin{matrix} X \\ \left[\begin{array}{l} m \\ \alpha \\ \beta \end{array} \right] \end{matrix} \quad (2.11)$$

In this equation, the vector δ contains all of the information for the waveform under observation and, therefore, needs to be recomputed for every new waveform; all entries of A are constants for a constant driving frequency and only need to be computed once; and the vector X contains all of the variables of the system. The individual solutions to this system of equations can be readily solved by using Cramers' rule [7]. These solutions are:

$$m = \frac{\det \hat{A}_1}{\det A}, \quad \alpha = \frac{\det \hat{A}_2}{\det A}, \quad \beta = \frac{\det \hat{A}_3}{\det A} \quad (2.12)$$

Where \hat{A}_n is a matrix formed by replacing the n th column of A with the δ vector. For α , the \hat{A}_2 matrix is

$$\hat{A}_2 = \left[\begin{array}{lll} \sum 1 & \sum f_n & \sum \sin(n\Delta) \\ \sum \cos(n\Delta) & \sum f_n \cos(n\Delta) & \sum \sin(n\Delta)\cos(n\Delta) \\ \sum \sin(n\Delta) & \sum f_n \sin(n\Delta) & \sum \sin^2(n\Delta) \end{array} \right] \quad (2.13)$$

The \hat{A}_3 for β is similar to \hat{A}_2 for α except the δ vector replaces the last column instead of the middle column. Only α and β are used to compute the magnitude of $\tilde{V}(t)$ which is given by

$$|\tilde{V}| = \sqrt{(\alpha^2 + \beta^2)} \quad (2.14)$$

The magnitudes of $|\tilde{V}_s|^2$ and $|\tilde{V}_c|^2$ are then used to compute the capacitance value using Eq 2.7.

The research of primary interest is water wave action, not tidal action. Therefore, the data of interest is data relative to an arbitrary reference point. For this reason, the mean (which shows tidal action) is of no interest at the present and is removed.

The fixed capacitor is included in the circuit to increase the effective range of water waves that can be measured by a capacitance wire and to maximize the change in voltage for a given change in water height. The relationship between the operating frequency, fixed capacitor, and fixed resistance are determined by calculating the transfer function of the circuit and plotting the magnitude of the capacitor voltage, V_c , as a function of frequency (Fig. 2.3). From this figure it is seen that there is a sharp drop off between $\omega RC = .5$ and $\omega RC = 1.5$ which will serve to maximize the change in voltage for a small change in ωRC . The point of maximum slope of this roll off is computed by taking the second derivative of the transfer function with respect to ωRC , setting it equal to zero and solving for ωRC . Performing this computation shows that the value of steepest slope is the 3 dB point of the curve, and occurs when

$$\omega RC = 1 \quad (2.15)$$

The value of the fixed capacitor is chosen so that the capacitance is equal to the assumed mean of the wire capacitance. The mean of the wire capacitance is the capacitance/meter of the enamel-coated wire multiplied by the mean submersion depth. This will maximize the range of water waves that can be measured because the variation in total capacitance will only change by a factor of two. This small change in capacitance will still keep the product ωRC on the linear portion of Fig. 2.3 with only small deviations on either side of the critical point.

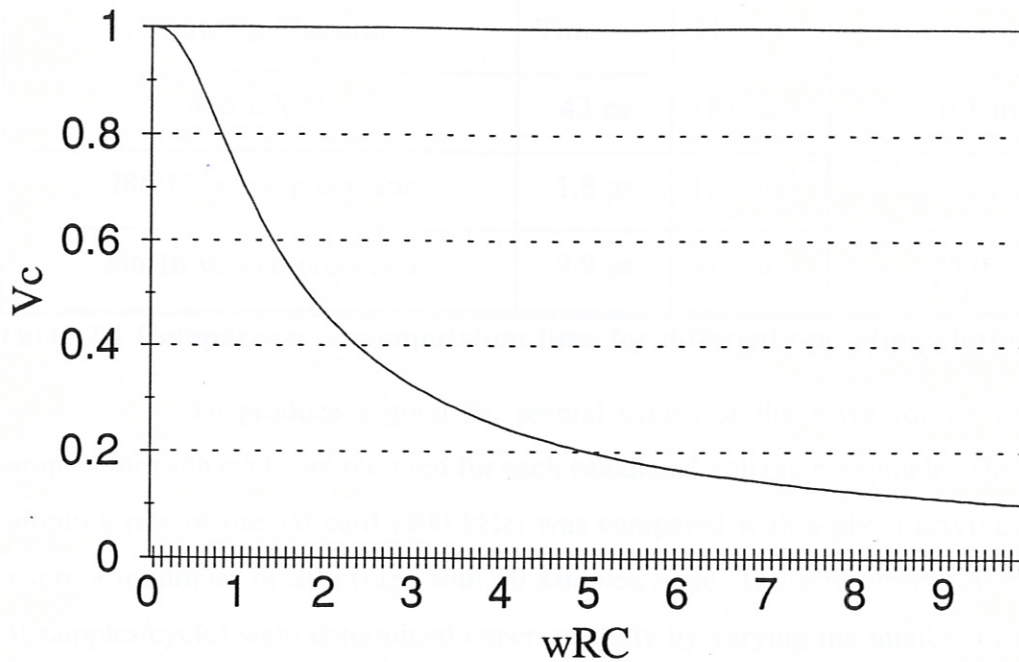


Figure 2.3 Output voltage vs. ωRC . ωR is constant, C changes.

The frequency of the driving voltage is determined by five different considerations. The first consideration was that the frequency be lower than the radiation frequency of the wires. The other considerations are the computation time, number of samples required to produce the minimum mean squared error, the speed of the analog to digital converter (A/D card), and the maximum frequency of interest in the wave field (Nyquist rate). The computation time required to produce the minimum mean squared error was simulated in software on three different operating platforms. The simulation program computed a known number of additions and multiplications. The execution of the program was timed and execution times for addition and multiplication were obtained (Table 2.1). The mean squared error algorithm requires 600 additions and 400 multiplications to produce one capacitance value. With these values and the addition/multiplication times, a minimum execution time was computed. The test was performed on a 486 DX/50, a 286/12 with math co-processor, and a 286/16 without a co-processor. The results of these three test are shown in table 2.1.

Operating Platform	Time/+	Time/*	Time/cap value
486 DX/50	43 ns	181 ns	0.1 ms
286/12 w/ co-processor	1.8 μ s	12.5 μ s	6.1 ms
286/16 w/o co-processor	9.9 μ s	47.7 μ s	25.0 ms

Table 2.1 Comparison of computation time for different operating platforms

To produce a good fit, several cycles of the wave forms, with several samples for each cycle are required for each calculated voltage magnitude. The maximum sampling rate of the a/d card (200 kHz) was compared with a given driving voltage to ensure a minimum of 20 cycles with 10 samples/cycle. These numbers (20 cycles with 10 samples/cycle) were determined experimentally by varying the number of cycles and the number of samples/cycle, and studying the change in standard deviation of the returned voltage. The numbers quoted above denoted the point of diminishing returns. That is, if these numbers are increased, the standard deviation of the measurement is not significantly decreased. Based on these numbers and the maximum sampling rate of the a/d card (200 kHz), an operating frequency of 10 kHz was used. This frequency is well above the Nyquist rate for the highest frequency component present in the wave field.

Knowing the operating frequency and total capacitance value, the fixed resistance is then chosen by solving for R from (2.15). This value is $R = 1/\omega C$.

2.2 Implementation of the Theory

Before discussing the implementation of the theory using electronic hardware and computer software, a section detailing the mechanics of the sensor is presented. Following this discussion, there are two sub sections detailing implementation of the theory.

2.2.1 Sensor Mechanics

The wire wave gauge sensor array consists of an array of vertical wires stretched over a mechanical frame. The small diameter wires are coated with a thin coat of enamel and one end is completely sealed with silicon. The voltage across the capacitor is digitized directly by an A/D card. From the digitized voltage measurements, the magnitude of the voltage is computed and a capacitance measurement is then obtained from the voltage magnitude.

Two different mechanical structures were designed and built for this project. The first was used for lab testing and initial deployment. The second is much bigger and permits simultaneous, two dimensional measurements of the wave field. Both of these designs are presented and discussed below.

2.2.1a One-dimensional "harp" array

The one-dimensional harp array was originally designed for test purposes in the laboratory. An illustration of this array is found in Fig. 2.4. It is small enough to fit inside of a 5 gallon bucket. This array consists of a 10.5" x 20" piece of plexiglass with a 8" x 13" piece in the center cut out. Along the top and bottom of the center section there are two 1" wide clamps also fabricated from plexiglass which are held in place by 9 bolts spaced at regular intervals. The clamps hold the ends of the wires in place. Eight 26 gauge enamel coated wires are placed so that there is a bolt on each side of the wire and all of the bolts on the bottom clamp are tightened. Each wire is individually stretched tight and the bolts on the top clamp adjacent to the stretched wire are tightened. The wire spacing for this array is nominally 2.5 cm. To be done properly, each wire has to be mounted sequentially. This method of fastening the wires is a serious drawback of this design. If one wire in the middle of the array works loose, all of the wires in the array have to be loosened and re-tightened. This method of wire mounting was consequently not used in future designs.

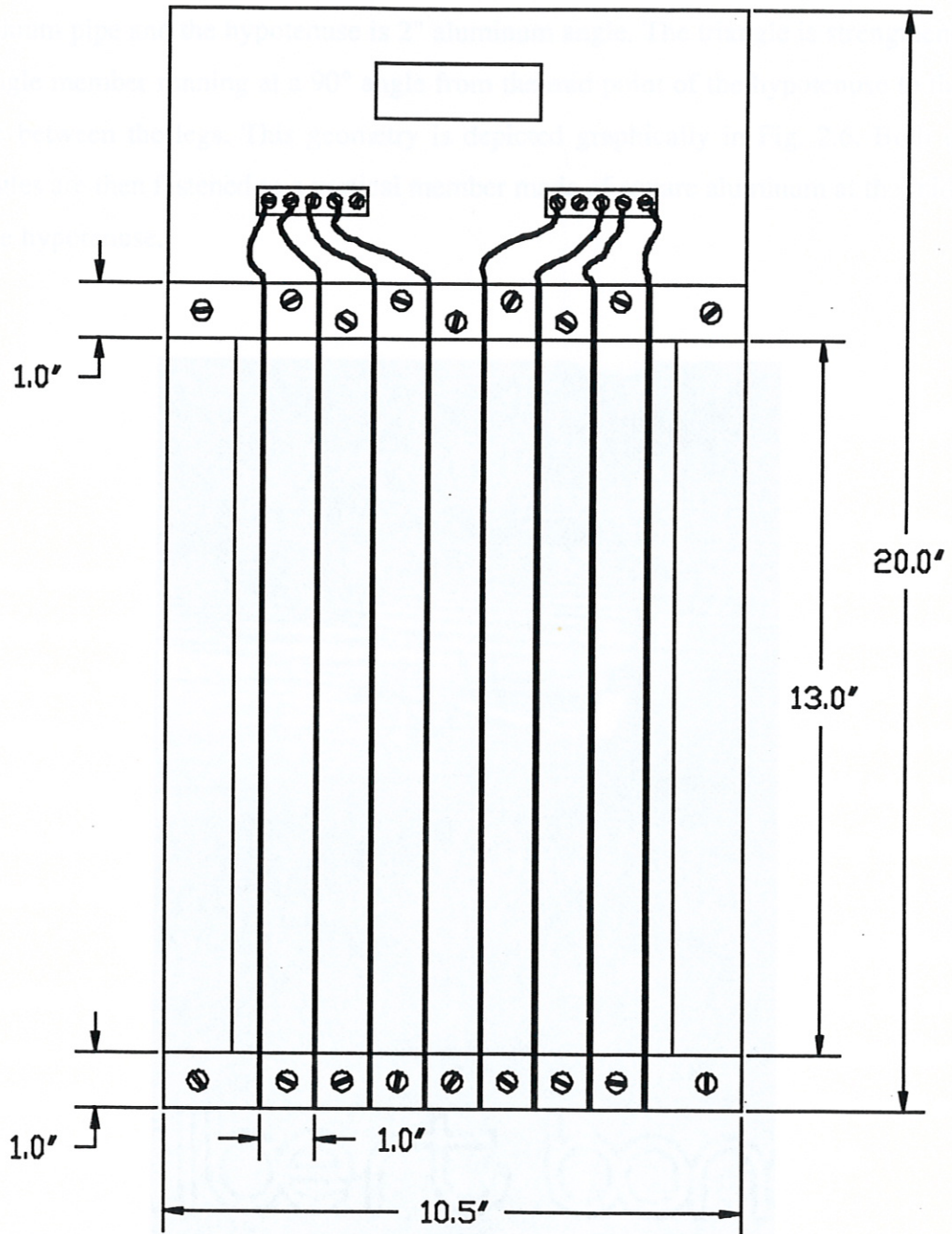


Figure 2.4 Small "Harp" array. Screw heads denote the area of the wire clamps.

2.2.1b Two-dimensional array

A two-dimensional array was designed and built after successful testing of the harp array. A picture of this array is found in Fig. 2.5. The top and bottom clamping points are isosceles triangles with 1 meter legs and 1.44 m hypotenuse. The legs are 1" aluminum pipe and the hypotenuse is 2" aluminum angle. The triangle is strengthened by an angle member running at a 90° angle from the mid point of the hypotenuse to the 90° angle between the legs. This geometry is depicted graphically in Fig. 2.6. Both of the triangles are then fastened to a vertical member made of square aluminum at the midpoint of the hypotenuse.

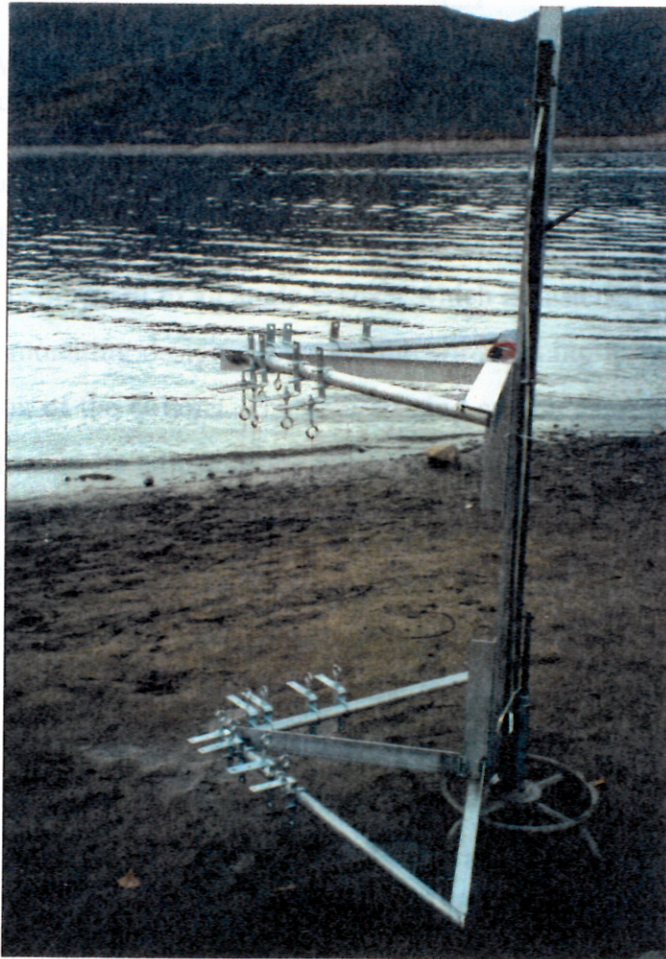


Figure 2.5 Large 2d array.

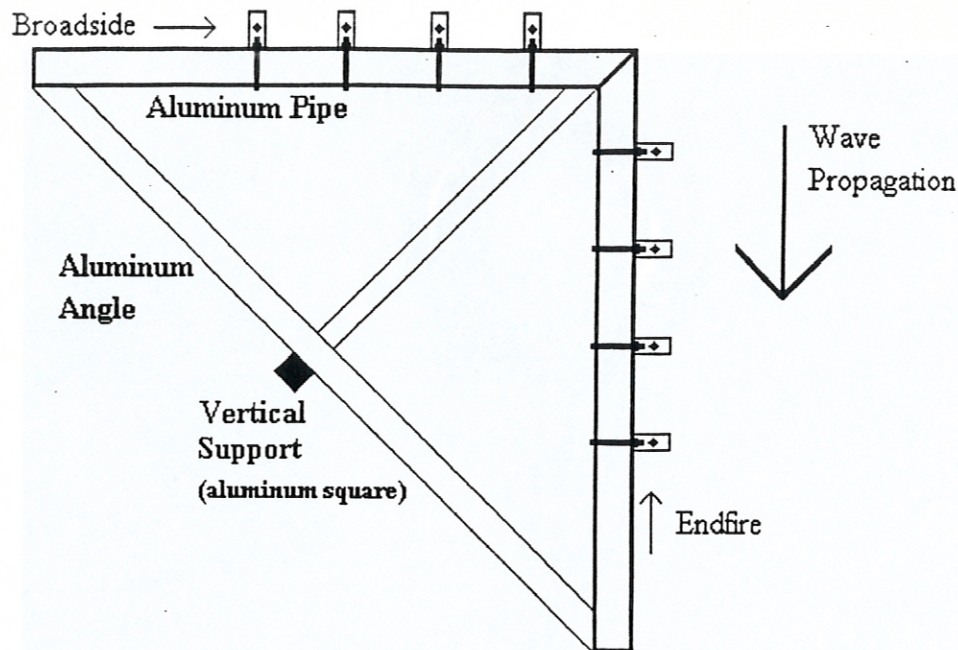


Figure 2.6 Top view of 2d array including wire mounting hardware and depiction of broadside and endfire directions.

The wires for the array (23 gauge) are fastened to eye bolts by wrapping the wire around the bolt several times and then wrapping the wire back onto itself. (Fig. 2.7) The eye bolt is mounted to an angle bracket which is fastened to the aluminum pipe by a U bolt. This mounting design allows for the wire spacing to be changed by merely moving the location of the U bolts. The wire spacing can be varied from 2.5 cm to 1 m. The wires are tightened by adjusting the nut on the eye bolt to the desired wire tension and then locking it in place by a second nut. This configuration of mounting hardware is depicted in Fig. 2.8.

This array allows for the simultaneous gathering of data in two orthogonal dimensions by placing wires on both legs of the array. By properly placing the array in the water, data can be simultaneously gathered for both broadside and endfire directions [8]. Broadside refers to waves that are propagating perpendicular to the array and endfire refers to waves that are propagating along the array as depicted in Fig. 2.6.

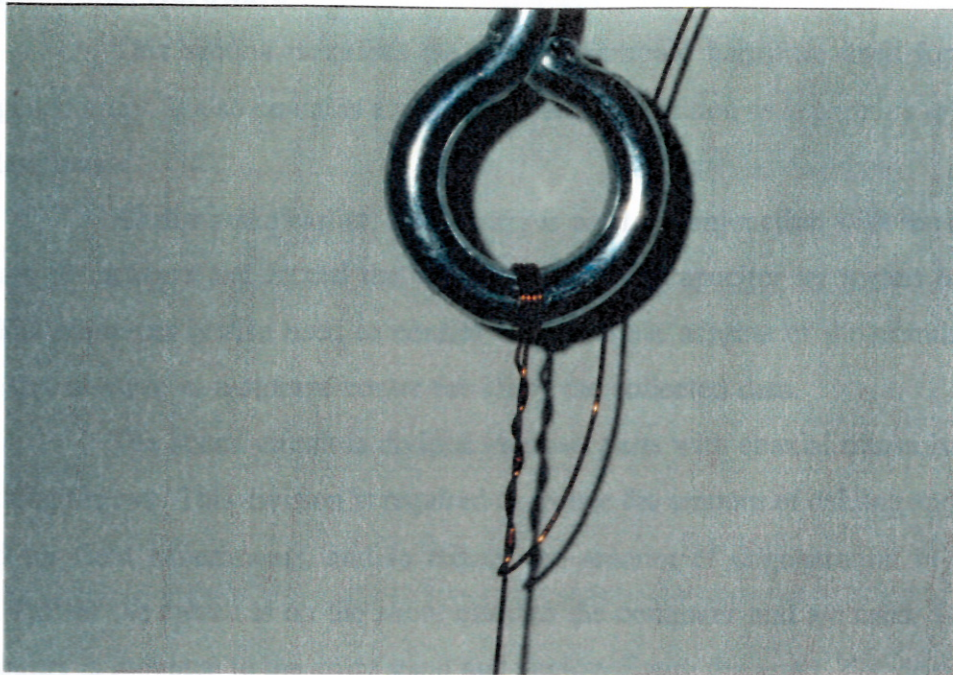


Figure 2.7 Anchoring of enamel-coated wire on eye bolts for 2d array.

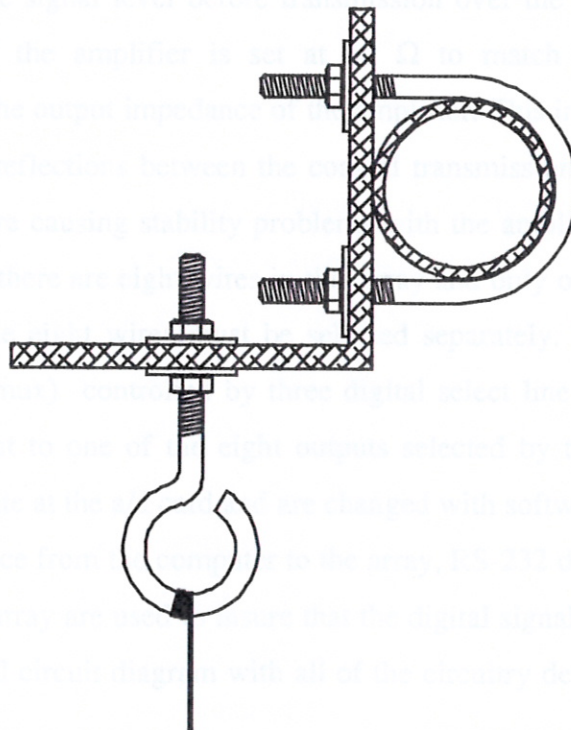


Figure 2.8 Wire mounting hardware for 2d array.

2.2.2 Electronic Hardware

This section describes the actual electronic hardware used for the wire wave gauge array. It also contains a section on data acquisition as it pertains to hardware considerations.

As discussed earlier, a computer is used in conjunction with the electronic hardware to measure and record the voltage across the capacitor by means of an A/D card. The computer is also used to control various other aspects of the circuit outlined below and to serve as a storage center for all of the collected data.

The actual circuit is divided into two parts with coaxial transmission lines connecting the two. This division is required to reduce the amount of cabling and circuitry needed for field experiments, and to reduce the amount of degeneration in the array signal. Part of the circuit is on the shore close to the computer and a/d card. The rest of the circuitry is mounted to the array stand and deployed with the array. The driving signal and the return signal for the circuit are transmitted to and from the array via the coaxial cables mentioned above. The return signal is passed through a unity gain buffering amplifier to boost the signal level before transmission over the long coaxial lines. The output resistance of the amplifier is set at 50Ω to match the impedance of the transmission line to the output impedance of the amplifier. This impedance matching was necessary to reduce reflections between the coaxial transmission line and the amplifier. These reflections were causing stability problems with the amplifier.

Since there are eight wires in this array and only one wire can be sampled at a time, each of the eight wires must be selected separately. To accomplish this, an analog multiplexer (mux) controlled by three digital select lines is used. The signal is passed from the input to one of the eight outputs selected by the digital address. The digital signals originate at the a/d card and are changed with software. To drive the digital signal the long distance from the computer to the array, RS-232 driver and receiver chips at the computer and array are used to insure that the digital signal will arrive undegraded at the array. The final circuit diagram with all of the circuitry described above is shown in Fig. 2.9.

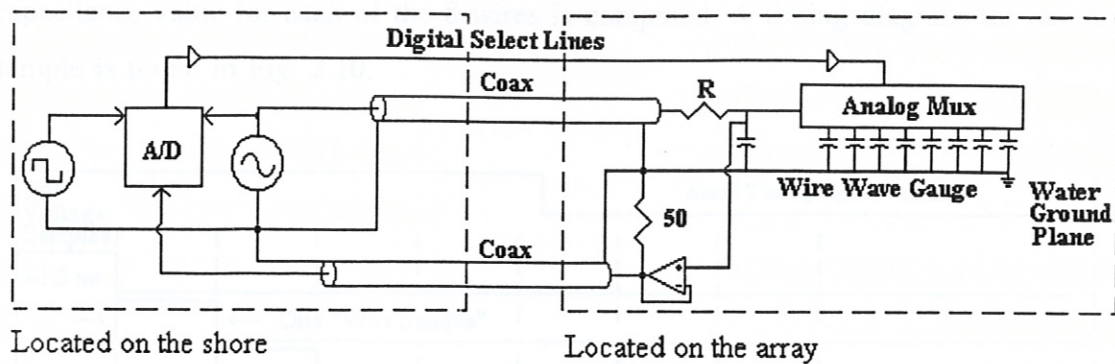


Figure 2.9 Electronic hardware diagram for wire wave gauge.

2.2.3 Software

The software for this system consists of programs which perform the minimum mean squared error to produce voltage magnitudes and compute the capacitance values using Eq. 2.7. Various techniques of making the data more interpretable are also implemented in software and will be presented in a later section.

To compute $|\tilde{V}_s|^2$ at the beginning of the data record, 5000 samples at 200 kHz are taken. For computing $|\tilde{V}_c|^2$ during the array scan only 300 samples are taken. There are more samples taken for $|\tilde{V}_s|^2$ because it needs to be very accurate, and the amount of time taken to compute it isn't a factor since it is computed before data acquisition begins.

As a basis for the following discussion on data acquisition, three terms are defined. 1) Voltage sample. "One digital voltage sample from one wire in the array. The sample rate being nominally 200 kHz" 2) Wire sample. "Collecting 300 voltage samples from one wire (approximately 1.5 ms). These 300 voltage samples are used to compute one capacitance value." 3) Array sample. "Sampling all 8 wires and performing data preprocessing. Data preprocessing converts the 2400 voltage samples (8 wires x 300 voltage samples/wire) to 8 capacitance measurements (one/wire)."

Ideally, all of the eight wires in the array should be sampled concurrently. However, due to hardware limitations, only one wire can be sampled at a given time. Thus, during a given array sample, each of the eight wires are individually sampled in sequence (Fig. 2.9) When all 8 of the wires have been sequentially sampled, the

capacitance value for each of the 8 wires is computed. A timing diagram for one array sample is found in Fig. 2.10.

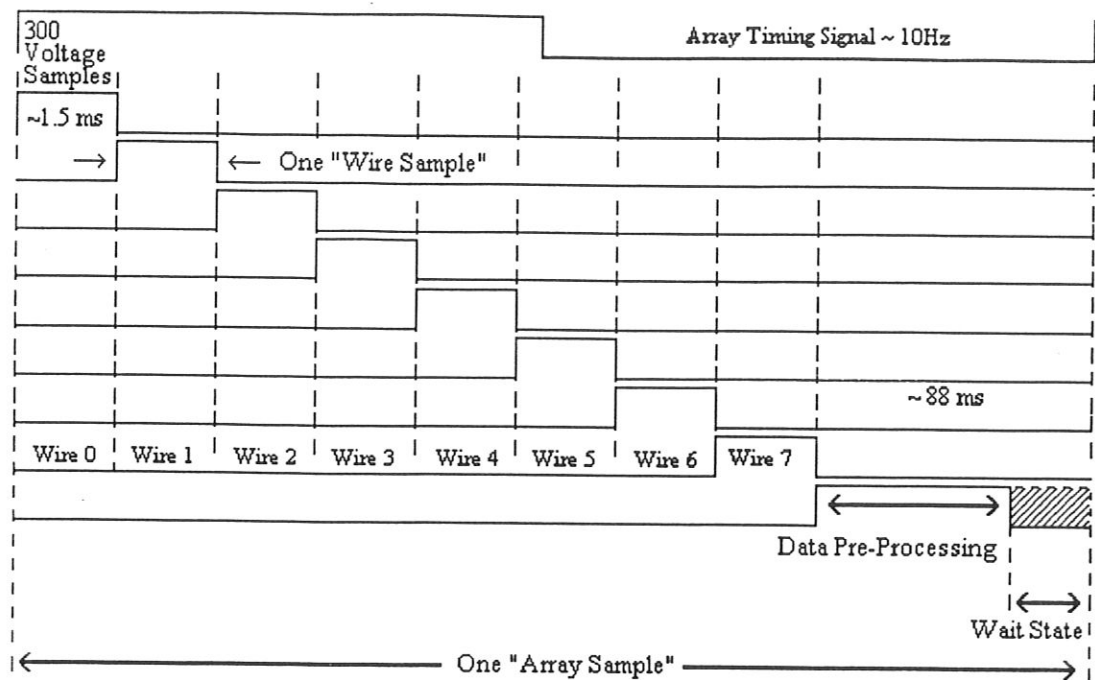


Figure 2.10 Timing diagram for one array sample.

2.2.4 Sampling Trigger

Each array sample has to be taken at uniform, discrete time intervals in order to accurately use the fast fourier transform (FFT) to analyze the spectrum. To provide extremely accurate separation between samples, the array sampling is triggered separately by an external clock. A hardware solution was chosen over a software solution to provide accuracy and robustness to the system. A second function generator is connected to one channel of the a/d card to provide the external trigger. The array timing is triggered by the rising edge of the 2nd function generator. This generator produces a square wave with a period just longer than the longest computing time for an array sample, as described above. The addition of the hardware trigger results in a fixed sample rate.

The frequency of the external trigger was determined experimentally by timing a data acquisition program while it gathered a specified number of array samples as fast as it could. The number of array samples divided by the elapsed time was the maximum frequency of operation. The frequency of the external trigger was then set slightly below this value to insure that the preprocessing always had enough time to finish before the trigger occurs. For the harp array, the maximum time was approximately .082 sec (12.2 Hz) and the trigger was set at .1 sec (10 Hz). It should be noted that the low frequency sampling of the array will limit the spatial resolution of the data. This will only be apparent when studying properties of the array, not properties of the individual wires which are samples at 10 kHz.

The data acquisition program for wave data collects 1050 array samples (8 capacitance values, one for each wire) in an array during data acquisition. This array is then saved to disk for further processing and analysis at a later date. The elapsed time between disk writes is approximately 1.75 min.

2.3 Instrument Performance

The resolution of the instrument sets the lower limit on changes in wave displacement that the array can accurately measure. The resolution is a combination of accuracy and precision. Accuracy is a measure of how close to the true value the computed value is. Precision is a measure of deviation between several values obtained from the same experiment. These two parameters can be illustrated by considering the results of a marksman shooting at a target. The mean distance from the shots to the bull's-eye is the accuracy. How tightly clustered the shots are is the precision. These parameters are limited by noise in the voltage measurements. The known noise sources that account for most of the noise in a given measurement are quantization noise from the a/d card, the algorithm for computing the capacitance, and fluctuations in the electronic hardware.

As a basis to discuss the accuracy and precision, a section on calibrating the data is presented. Following the calibration section, two sections on accuracy and

precision are presented. They describe several different tests which were performed to quantify how well the instrument is working.

2.3.1 Instrument Calibration

The data collection algorithm described previously, returns a capacitance value which is proportional to the height of the water. To be able to evaluate the data, height values are desired. To obtain height data from the capacitance measurements, calibration data is taken when the array is submerged a known water depth. For the harp array, the data is collected in a level 5 gallon bucket for several different water heights. For the 2d array, the data is collected at several different heights relative to the array stand. For calibration data, a total of 1000 capacitance values were collected for each wire and averaged to obtain one very accurate capacitance value which corresponds to a known water height. Calibration data (instead of Eq. 2.1) is used to correlate capacitance values to water height because stretching the wire changes the diameter of the wire, and the method for applying the enamel to the wire produces non-uniform enamel thickness. Therefore, to use the formula, one would need to replace the values for the diameters with functions that describe the diameters.

In the post collection data processing, the data analysis software first takes the file of calibration data, fits the calibration points to a straight line using a least squares algorithm, and computes an offset and slope for each wire. The linear fit of the calibration points is of the form

$$\eta(cm) = a_0 C(nF) + a_1 \quad (2.16)$$

where a_0 is the slope of the calibration line in cm/pF and a_1 is the offset value in cm. Typical values for these two parameters are .005 cm/pF and .5 cm. A comparison of the calibration data and the linear fit is found in Fig. 2.11. This plot contains both the raw calibration data and the straight line formed by using the height, slope and offset data in Eq 2.16. Slope and offset values are calculated for each wire so that the height value returned from each wire will be exactly the same for a given water height.

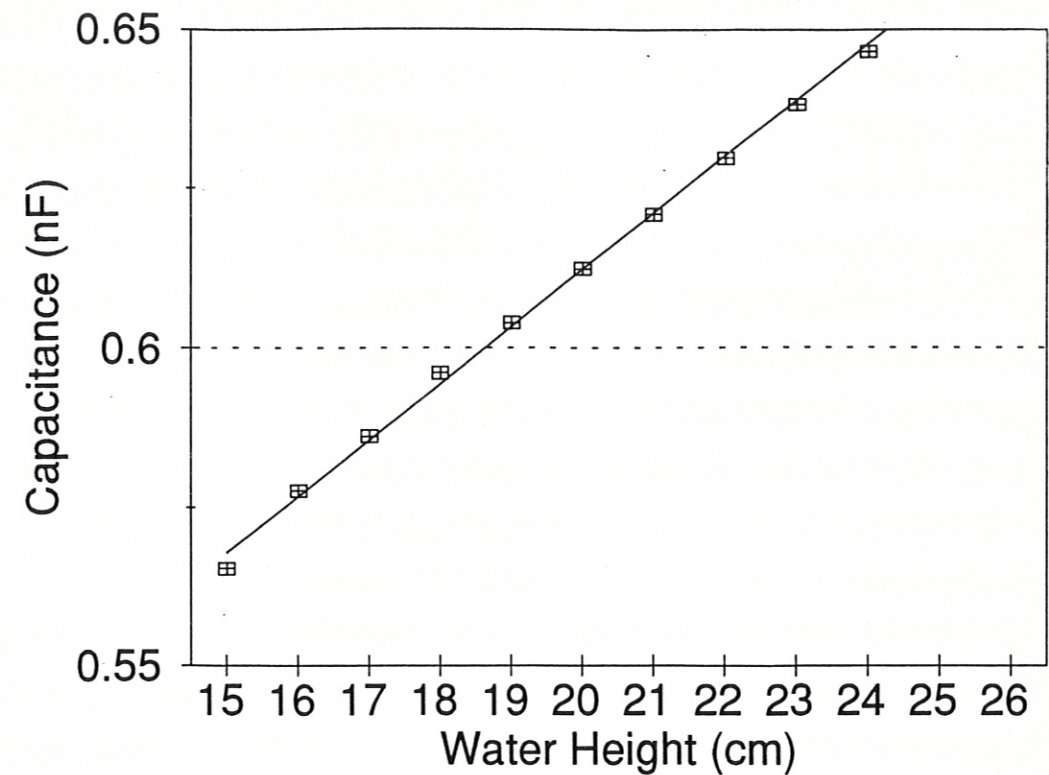


Figure 2.11 Calibration data vs. linear fit.

The capacitance data is read from disk, converted to height in cm, and stored in an array. The average of this array is then computed and subtracted from each element of the array. This latter process is termed "removing the mean". The result is a time series of water wave displacement in cm for each wire (Fig. 2.12).

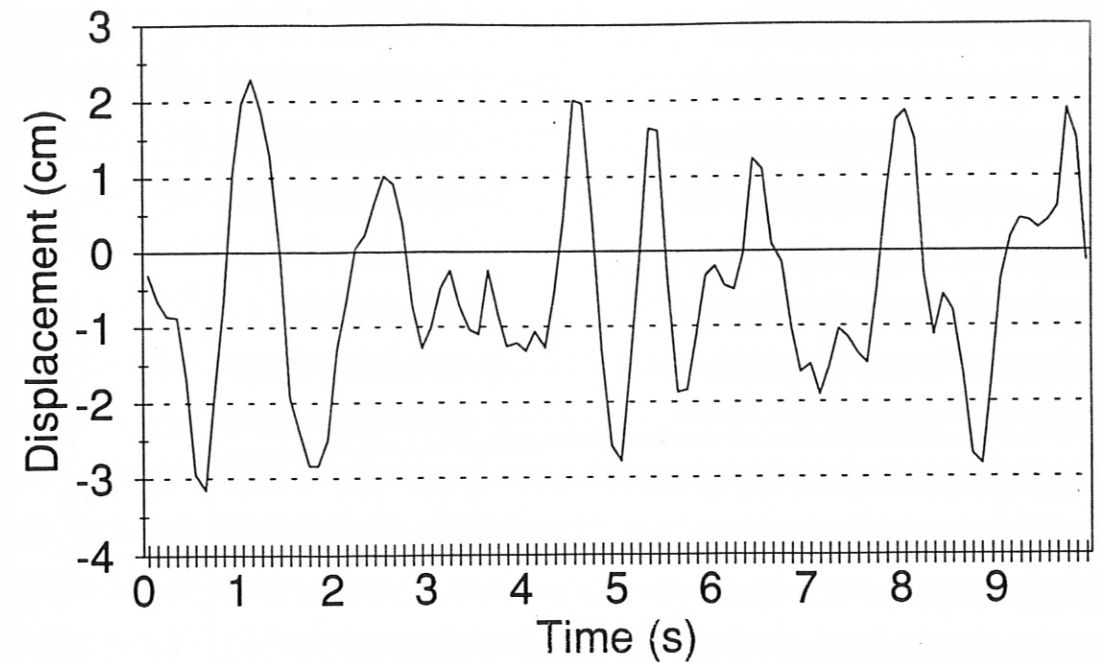


Figure 2.12 Typical time series of water wave action.

2.3.2 Accuracy

The accuracy of the instrument is dependent on how close to the true wave height a given measurement is. An evaluation of the measurement accuracy was determined by placing the harp array in a bucket of water where the water height was known. Calibration data was then taken to correlate the capacitance measurements with the water height. The water for the calibration data was allowed to settle for ten minutes between calibration points to obtain the most accurate values. A data set was then taken in the still water, and the average water height in cm was calculated. The difference between the calculated average and the actual water height is the measured accuracy of the instrument. The individual averages were plotted from several consecutive data records to show a time series of the average height and to evaluate possible instrument drift.

Because of concerns over function generator stability, the tests were repeated again using a much more stable function generator for the driving frequency. The time series of this last test is shown in Fig. 2.13. This figure distinctly shows a

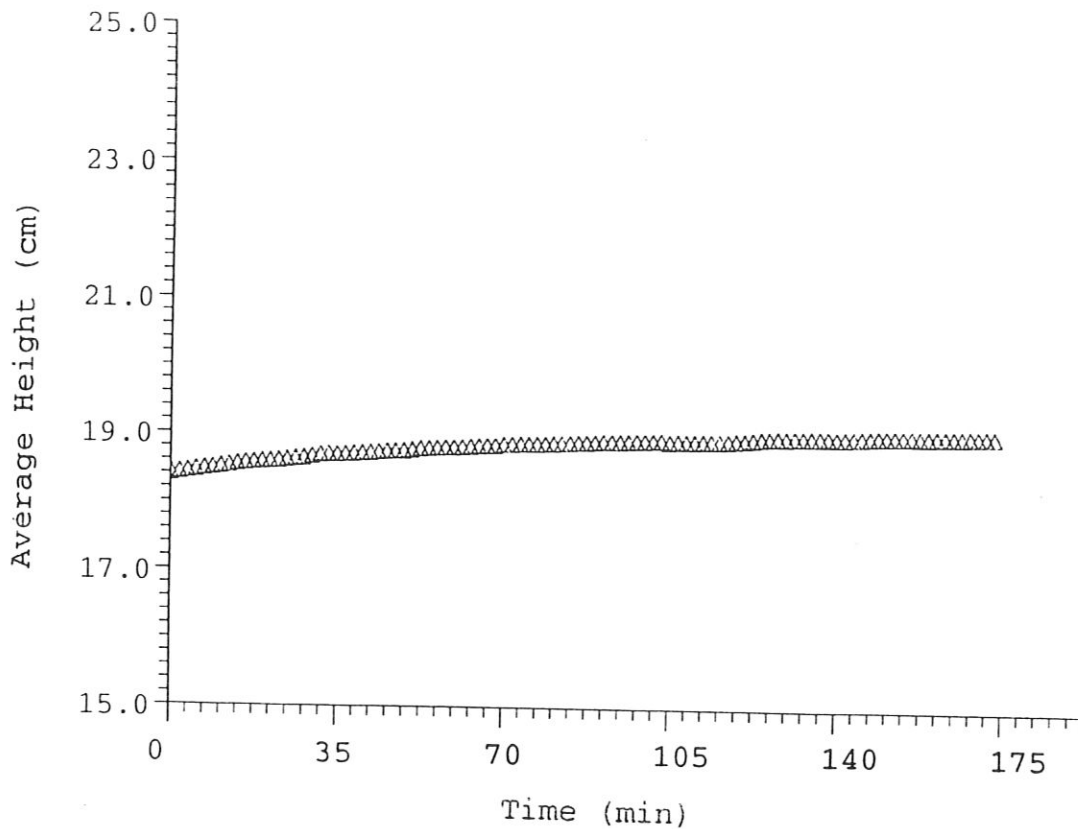


Figure 2.13 Time Series of the average water height on still water.

deviation in the average height as a function of time. Further research on this drift proved that the accuracy drift was caused by a temperature dependent drift in the output of the line buffering amplifier at the array. When the amplifier had been on for several hours, the drift stabilized. This drift in the accuracy produces no effect in the analysis of the data because, as mention earlier, the mean is removed from the data at regular (approximately 1.75 min) intervals. Since the drift in accuracy appears in the data as a drift in the mean, removing the mean also removes the drift in the accuracy. Thus, accuracy is limited mainly by temperature drifts in the electronic hardware.

2.3.3 Precision

When several different measurements are taken under identical situations, there will be some difference between each of the measurements. This deviation is the precision of the array and can be thought of as how repeatable any given experiment is in terms of gaining the same value from identical surrounding conditions. To examine the preciseness of the wave gauge data, the same data used to produce the time series for accuracy was manipulated to produce a 3 hr time series of the standard deviation for still water. Each data record that made up the time series was taken immediately following the previous one so that the conditions stayed essentially constant from one record to the next. This plot is found in Fig. 2.14. Each point in the figure represents the standard deviation of 1024 capacitance measurements. The distance between the points is roughly 1.5 min. The still water mean standard deviation as shown by this plot, is approximately .1 mm. Based on this number and the flatness of the plot, it was concluded that the precision of the instrument is very good.

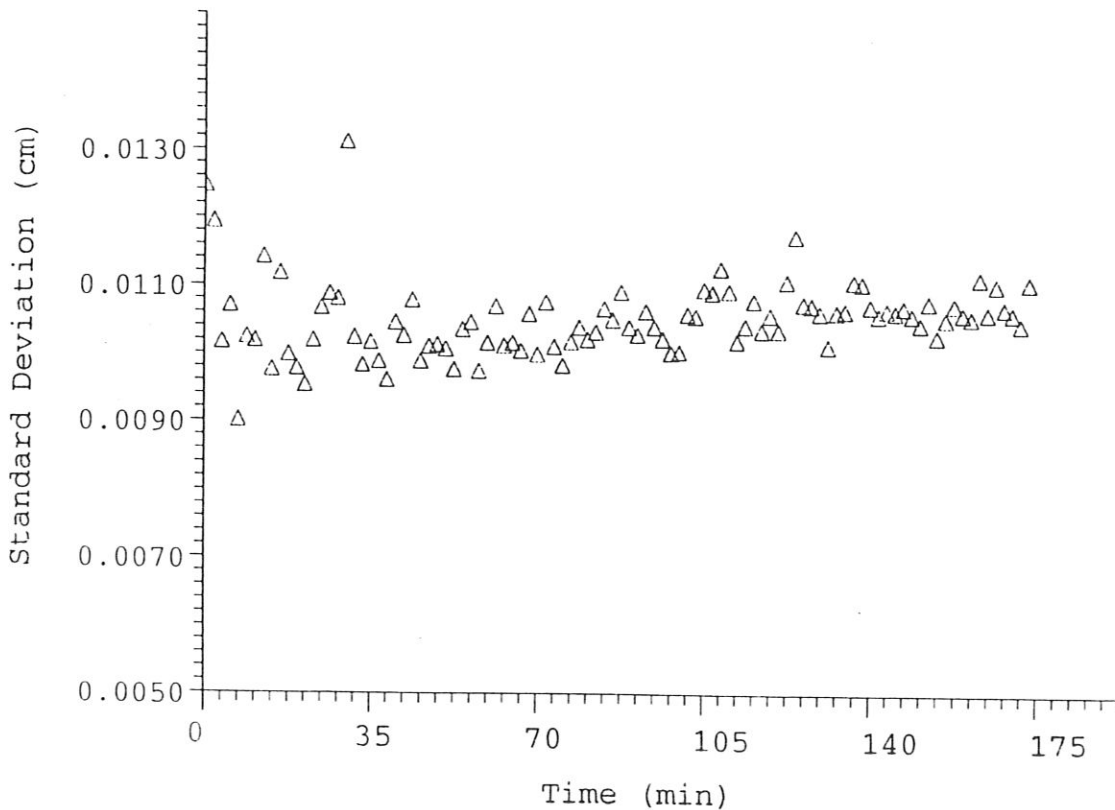


Figure 2.14 Time series of standard deviation in still water.

In an attempt to study the dynamic response of the array, a second 1 hr set of data was gathered for water that was being agitated by a small electric mixer. The standard deviation and average height were then plotted as a time series. This plot is found in Fig. 2.15. This plot of the agitated water shows that the process of agitation produced a variation in the standard deviation that remained essentially constant. Again, the flatness of the plot shows that the array is quite precise.

The precision is, therefore, limited mainly by the stability of the driving frequency. However, precision will also be limited by the quantization noise of the a/d card. The quantization noise from the a/d card can be minimized by maximizing the magnitude of the input voltage so that more bits of the card are being used to compute the voltage. This noise is further minimized by the use of multiple samples to compute one capacitance value [9].

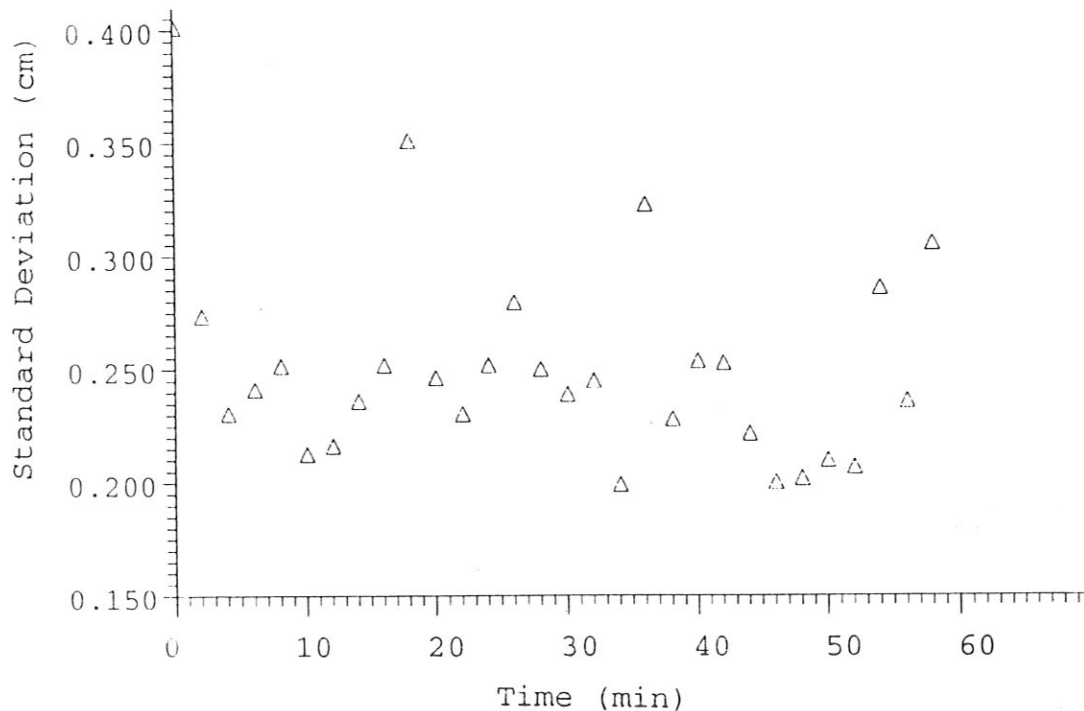


Figure 2.15 Time series of standard deviation in agitated water.

As mentioned earlier, there were concerns about the stability of the driving frequency and its affect on the precision. It was found that the software algorithm was quite sensitive to variations in the driving frequency. This sensitivity is verified by comparing the 1st and 2nd halves of Fig. 2.16. The first half is the standard deviation for data that was taken using a Hewlett Packard 3310A Function Generator to generate the driving frequency. Significant deviations in the output frequency for this unit had been observed during previous lab experiments. The second half is for similar data that was taken using a Hewlett Packard 8904A Multifunction Synthesizer (a very stable frequency generator). This unit displayed extreme accuracy in maintaining a given output frequency. A careful comparison of these two plots shows that the standard deviation in the noise measurement was decreased by one order of magnitude just by using a stable oscillator for the driving frequency. This moved the precision (mean standard deviation) of the array from .96 mm to approximately .10 mm.

To investigate how accuracy is affected by wire tension, the accuracy and precision experiments described above were repeated for four different wire tensions. As discussed earlier, the wires for the harp array are individually tightened and clamped in place. This method of tightening and clamping the wires makes it difficult to directly measure the wire tension other than the relative pitch the wire produces when plucked in the center of the array. The four wires used in the experiments were categorized as tight, moderately tight, loose and very loose. The fixed capacitor was also sampled by removing one of the wires from the array and selecting that "wire" with the mux to be sampled. Removing the wire from the array eliminated any fluctuations in the water that might be present. The results of this test showed accuracy was essentially unaffected by wire tension. These results are shown in Fig. 2.17 and Fig. 2.18. Figure 2.17 is the precision and accuracy for tight wires using the same two function generators described above. Figure 2.18 is for loose wires. The differences between tight and loose wires are insignificant.

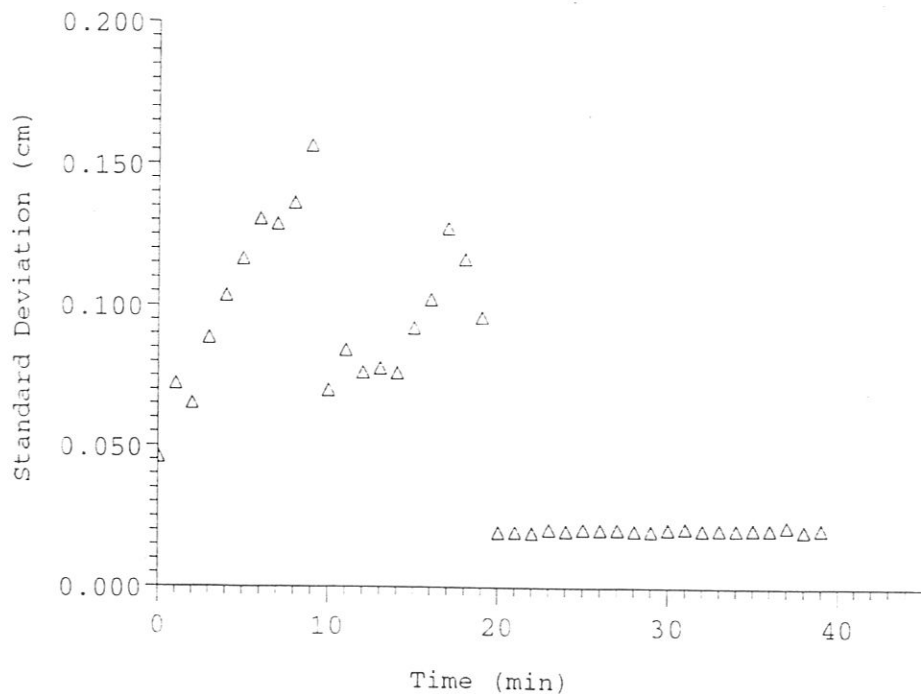


Figure 2.16a

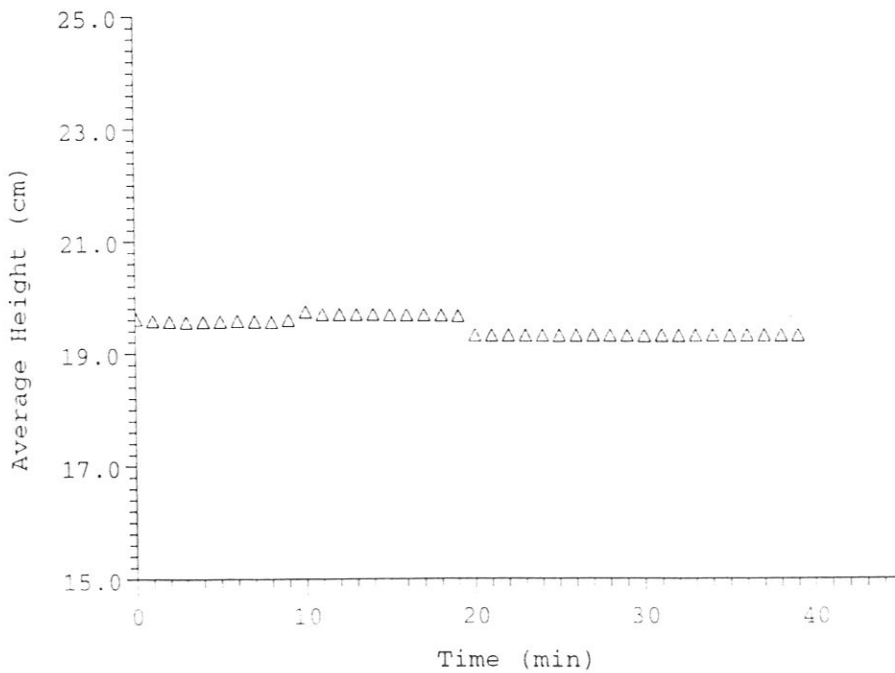


Figure 2.16b Time series of Precision (a) and accuracy (b) for tight wires. The first half of the plot is data taken using the less stable driving frequency while the second half is using a much more stable source.

From the tests describe above, it was concluded that the algorithm is extremely sensitive to variations in the driving frequency which decreases the precision; wire tension doesn't significantly affect either accuracy or precision; and there is a temperature dependent drift in the line buffering amplifier that causes a slight drift (.25 cm to .9 cm) in accuracy over time. This drift does not affect the analyzed data, however, because the mean is removed from the data before it is processed.

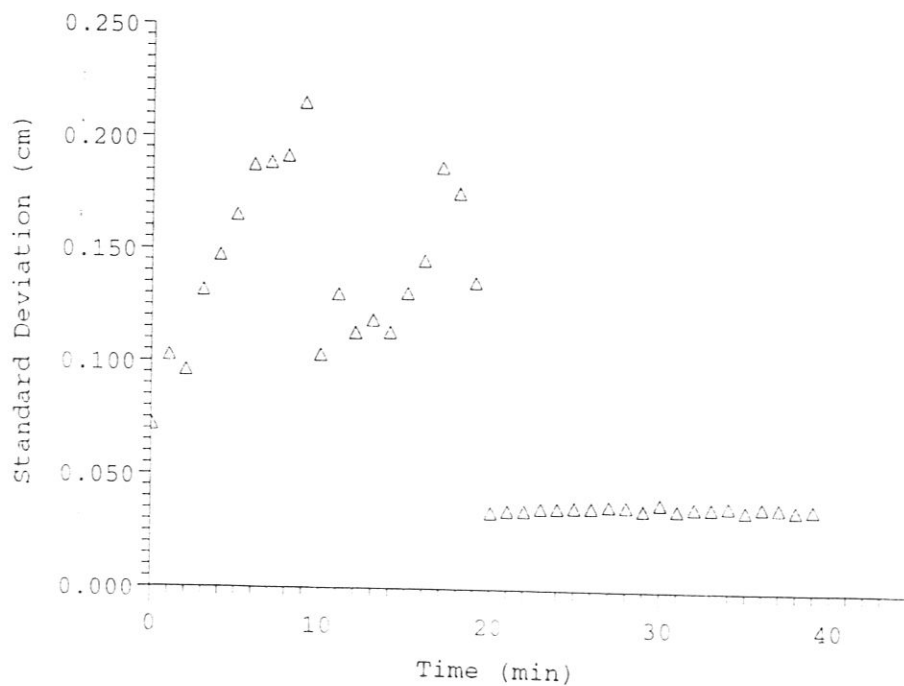


Figure 2.17 Time series of precision for loose wires.

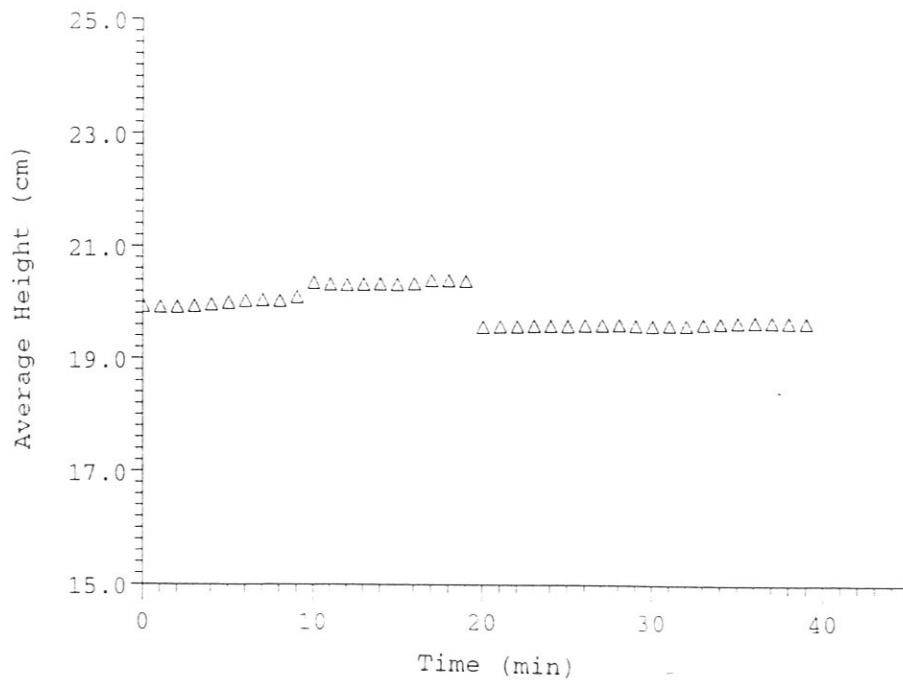


Figure 2.18 Time series of accuracy for loose wires.

FIELD DEPLOYMENT

When the design of the "harp" array was completed and preliminary tests were concluded to verify basic functionality, the array was deployed in the field at two different sites away from the laboratory to study wind generated waves. During these deployments, a weather station that recorded wind direction and speed, and air temperature was also deployed. This section describes the preliminary planning for the deployments, what was gained from each major deployment and results that demonstrate functionality of the array.

3.1 Preparation for Deployment

Before the initial deployments, a detailed list of the equipment needed for the field experiments was developed and an preliminary visit to each site was made to ascertain where the equipment would be set up and how much cabling would be needed to complete the experiments. To manage the enormous amount of equipment and insure that vital equipment was not left behind, the equipment list was divided into logical sub groupings. These groupings were: power, cabling, computer software, array, weather station, tools, personal and miscellaneous. One important area to include was backup cabling and equipment in the case of failure. This area included a backup of all executable and source code and a backup of system files on floppy disk. Having the system files on floppy will allow the experiment to proceed in the event that a hard disk is damaged enroute to the test site. After an initial draft of the equipment list was completed, the list was presented to other individuals acquainted with the project for their input on other items not listed. To further facilitate organizing the smaller pieces of equipment, two large plastic boxes for packing the cabling and the small equipment during transport were obtained.

Power for the field experiment was provided by a 4 kW gasoline powered generator. The ac output of the generator was passed through a saturable core voltage regulator. This was used to establish a proper operating voltage and to suppress surges from the generator. Before the power reached any of the equipment, it was passed through surge suppressors for further regulation. It was found that the voltage regulator produced significant electric fields that effected the operation of the computer monitors. Because of this phenomena, the regulator was placed several feet from any of the equipment.

On the day of the field experiments, all of the equipment on the list was carefully packed and the list was double checked to insure that all of the items on the list were included. Each member of the deployment team was assigned a list of equipment that they were responsible for packing and getting to the vehicle.

The first order of business after the equipment was set up and properly operating at the test site was to gather calibration data. For the harp array, this data is taken on a nearly level, still bucket of water on the beach for several different water heights. For the large 2 dimensional array, the array is clamped to the stand at different heights in the water. Several samples are taken and averaged to get a usable value for each depth. The calibration data is taken and fit linearly to obtain a slope and offset for each wire. Having this data allows us to produce height instead of capacitance values.

The wind data from the weather station was a running 5 min average stored to disk every 30 sec. It was desired to have accurate wind data for the entire length of the experiment. Since the weather station usually required less setup time than the wave gauge, wind data collection could start 5 - 10 min before any wave data was taken. The weather station used a separate computer for operation and data storage. This computer and the computer for the wave data were set to the same time and all of the data was time stamped so that they could be compared at future dates. The anemometer was deployed on top of the deployment vehicle. The height above the ground was nominally 10 feet.

After the calibration data was taken, actual data records were collected. Each data file contains ten two minute records taken at regular intervals. While the data

is being collected the field personnel make notes in notebooks that will assist in making the experiment repeatable.

When the experiments are completed, all of the data is backed up on floppy disks and the equipment is repacked into the vehicle. When everything is loaded, there is a final inspection of the area to find anything that might have been missed and to police the area for trash. All of the data analysis takes place in the lab.

3.2 Major Deployments

Our first deployment site was at the end of the south quay at Utah Lake State Park. (Fig. 3.1) Because the water level was very low, extra cabling had to be used to transmit the signal from the computer to the array. The total distance between the computer and the array was 100 feet. At this distance, the water was only about two feet deep. The wind for this first deployment varied from slight to non-existent. Because there was no wind, there were no waves generated on the surface of the lake. In an effort to gather some data, two members of the deployment team entered the water with large pieces of plexiglass to mechanically generate some waves. (Fig. 3.2) This action did produce fluctuations in the data, but didn't show if the instrument was working because the spectrum of the data could not be interpreted. The deployment was labeled as a success, however, because we were able to get out to the field and deploy without forgetting or breaking any equipment. We used this experiment to evaluate equipment and plan for other field experiments.

Subsequent deployments were on a shallow beach at the Island Resort at Deer Creek Reservoir. (Fig. 3.3) At this deployment site, the vehicle was able to be driven to the edge of the water. (Fig. 3.4) With 50 feet of cabling between the computer and the array, a water depth of roughly three feet at the array was obtained. Deer Creek Reservoir is located in a canyon such that there is usually wind every afternoon. This proved to be true for two of the three deployments that were made at Deer Creek.

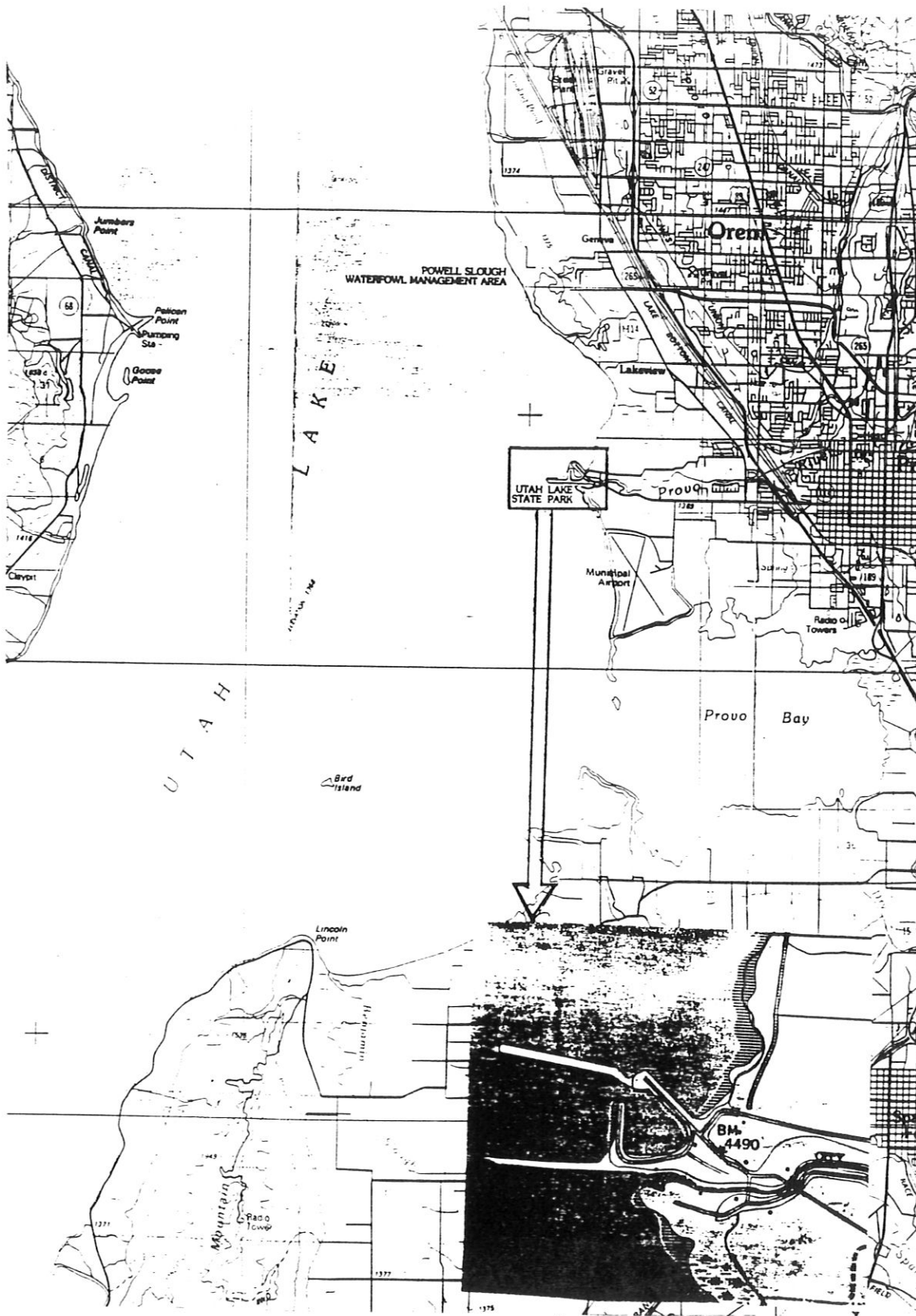


Figure 3.1 Deployment site at Utah Lake



Figure 3.2 Mechanical generation of waves at Utah Lake.

3.3 Deployment Results

The first two deployments at Deer Creek Reservoir were conducted in identical manner and provided similar information. Both provided wind and wave data. The wave data was processed to produce the wave spectra of the water in time. Figure 3.5 shows the wind wave spectra from one data record taken on the first deployment. The roll off of this spectra, when plotted in log-log space(as shown) should be approximately a straight line with slope -5 [10]. This is shown by the straight line fit of the data, also in this plot.

Based on the spectral results it was determined that the instrument was providing the desired information on wind generated water waves. The next task was to verify that the information being gathered by the array was in fact wind generated waves. Two analyses of existing field data were performed to verify that the data was in fact wind waves. These two analyses were to study the peak frequency of the

Figure 3.3 Deployment site at Deer Creek Reservoir

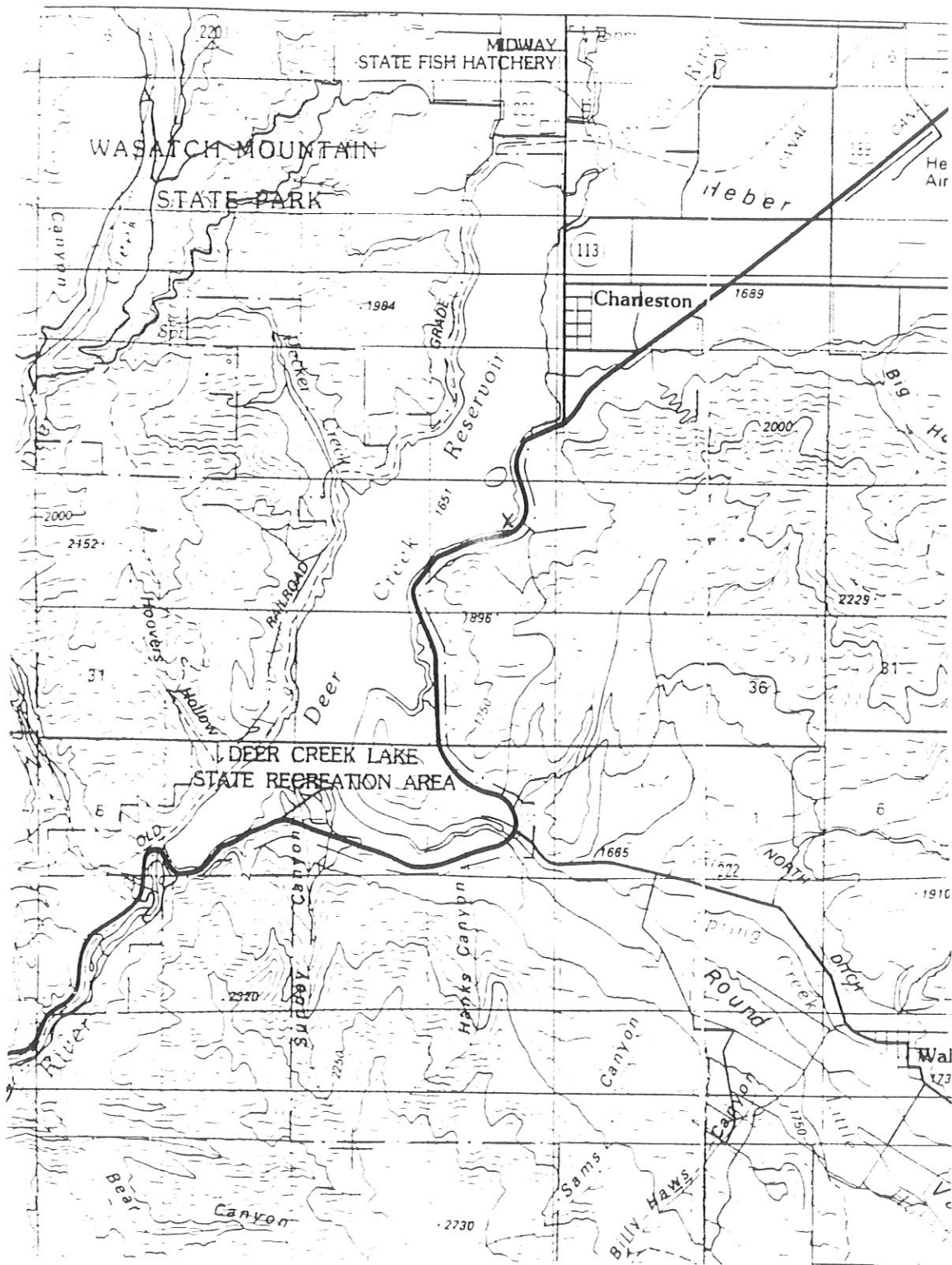


Figure 3.3 Deployment site at Deer Creek Reservoir



Figure 3.4 Photo of deployment site at Deer Creek Reservoir

spectrum as a function of wind speed, and the variance of the data versus the wind speed.

As the wind increases over a body of water, the waves generated become larger in size and lower in dominant frequency. That is, the dominant frequency of wind generated water waves are inversely proportional wind speed. Figures 3.6a and 3.6b show a visual comparison of the difference in dominant frequency for two different wind speeds. The difference is most noticeable by comparing the relative amplitude of the waves, and the existence of breaking waves. The change in dominant frequency is seen as a shift of the peak of the power spectrum. The plot of the power spectra from data taken at the same time as the pictures is shown in Fig. 3.7 and 3.8. Comparison of the two spectra displays a shift in the spectrum.

To further illustrate the variation in frequency as a function of wind speed (using wave gauge data) Fig. 3.9 is a scatter plot of wind speed versus dominant frequency of the power spectrum for different deployments. The parameters for the linear fit are $a_0 = -0.0287$ and $a_1 = 0.159$. Each of the deployments used to gather

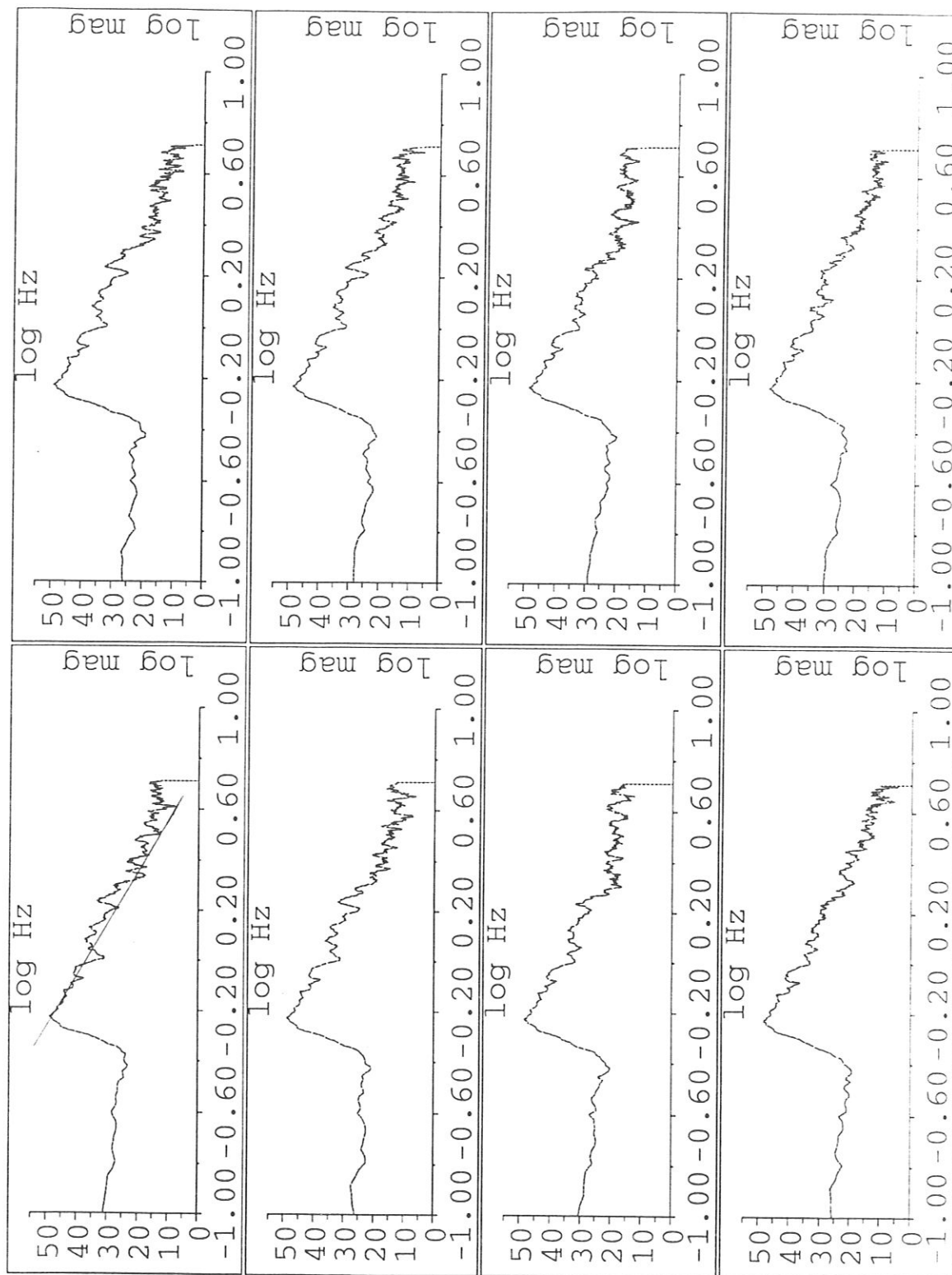


Figure 3.5 Power spectra for wind generated water waves. Each window represents one wire in the array. The regression line on the first window represents the theoretical roll off.



Figure 3.6a

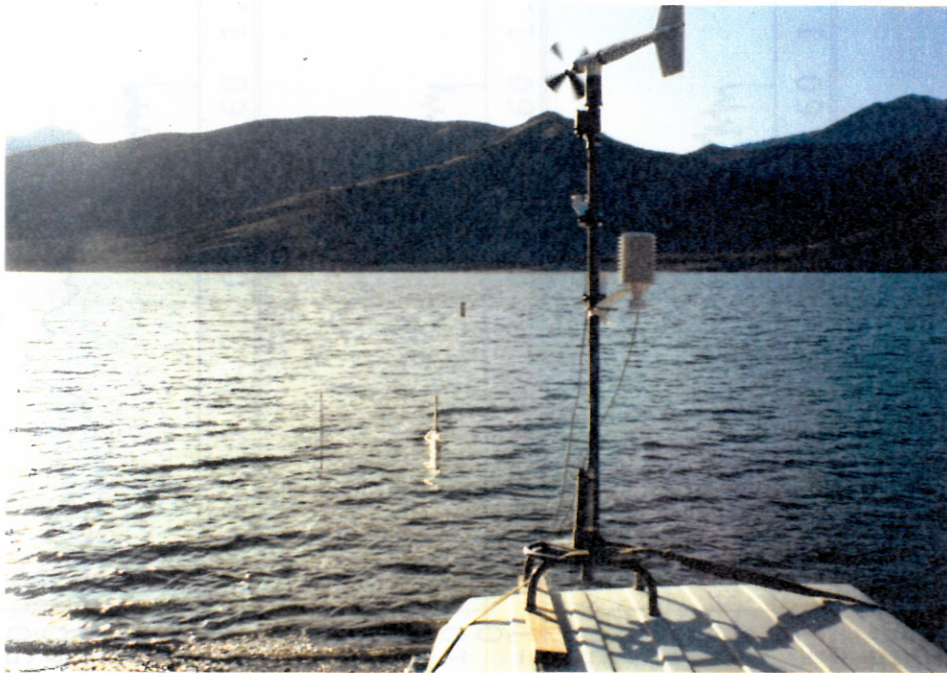


Figure 3.6b Comparison of dominant wave frequency for high wind speeds (a) and low wind speeds (b).

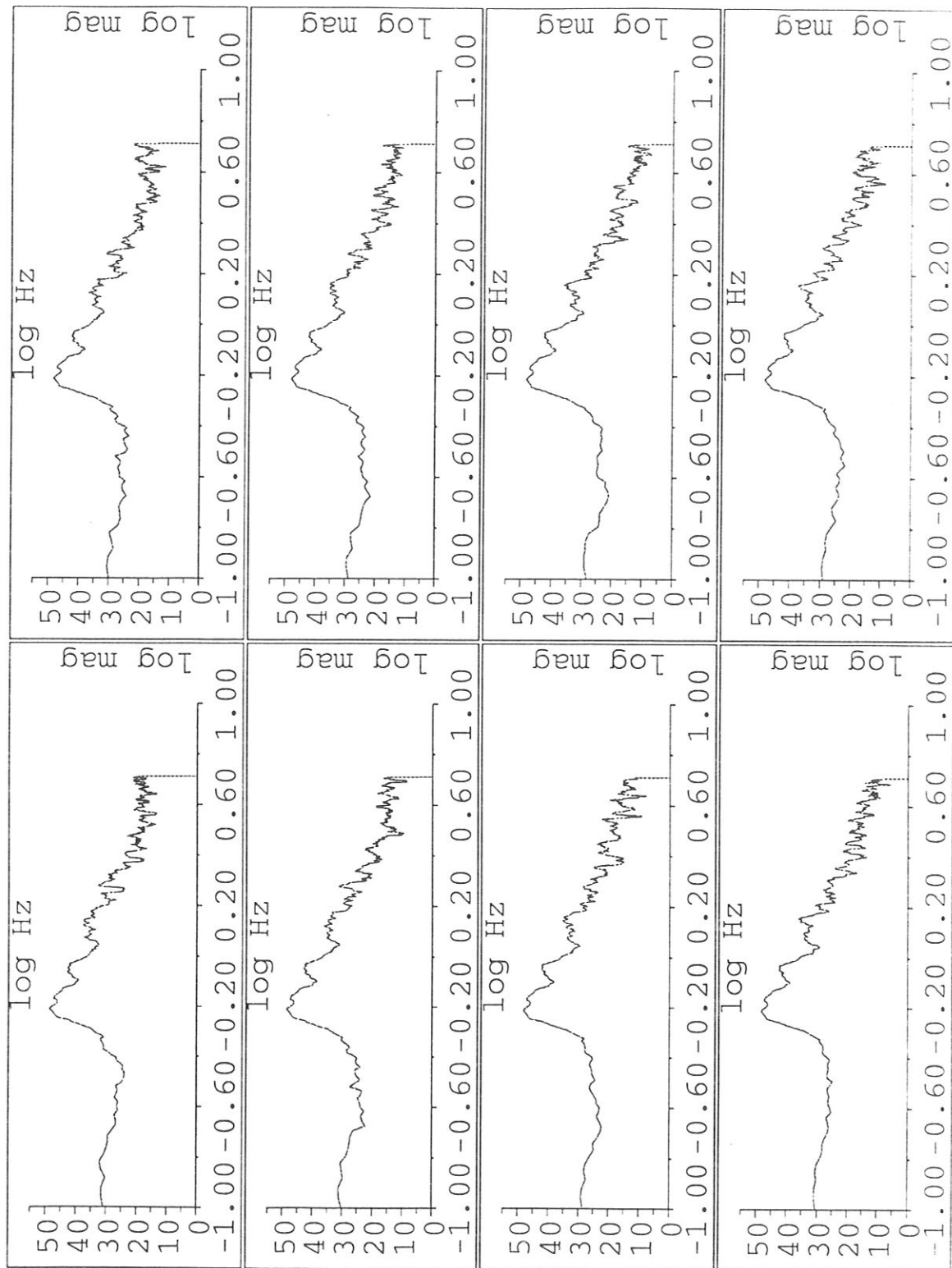


Figure 3.7 Power spectra for high wind speed. Data taken at Deer Creek Reservoir October 6, 1992.

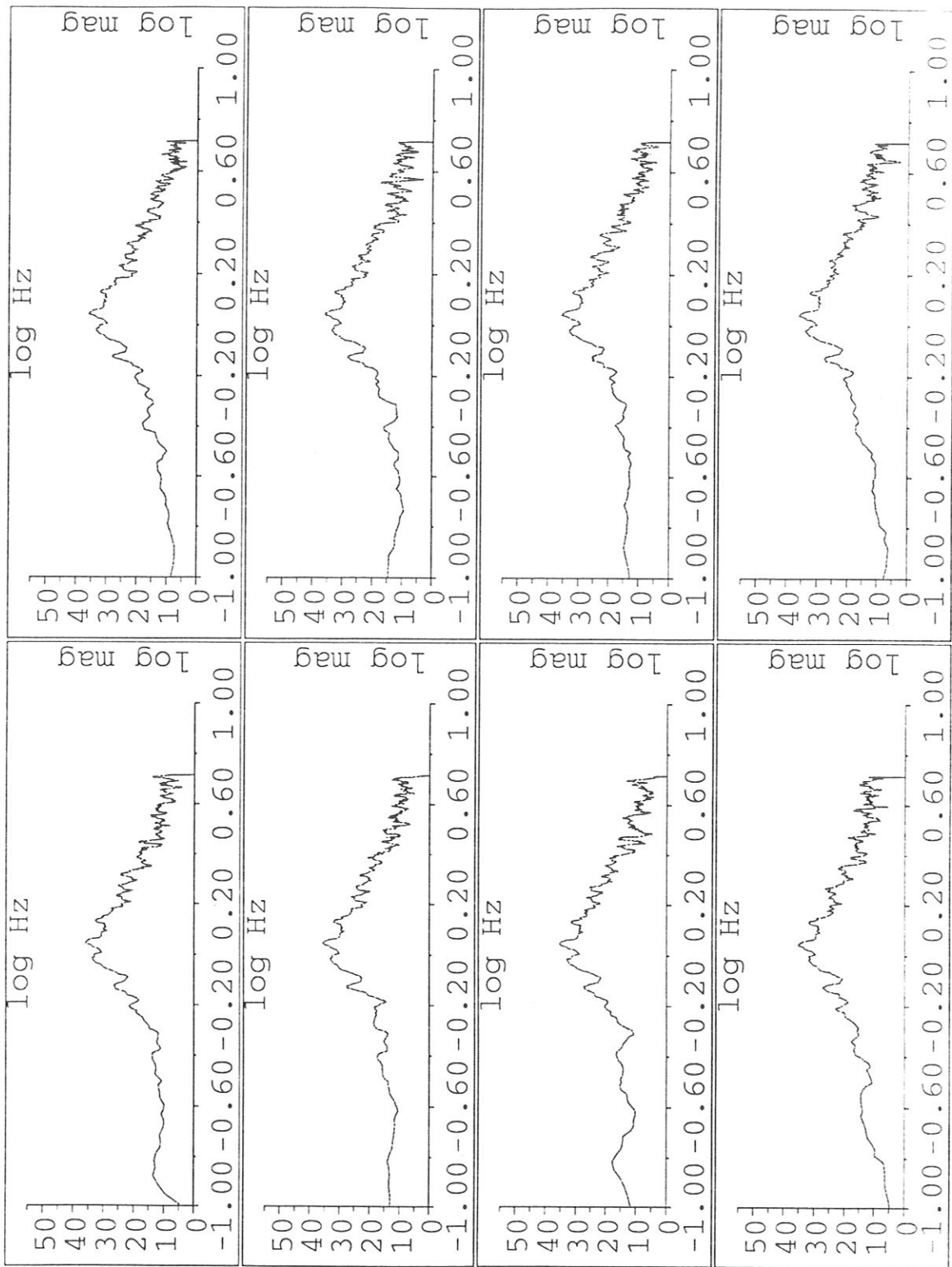


Figure 3.8 Power spectra for low wind speed. Data taken at Deer Creek Reservoir September 30, 1992.

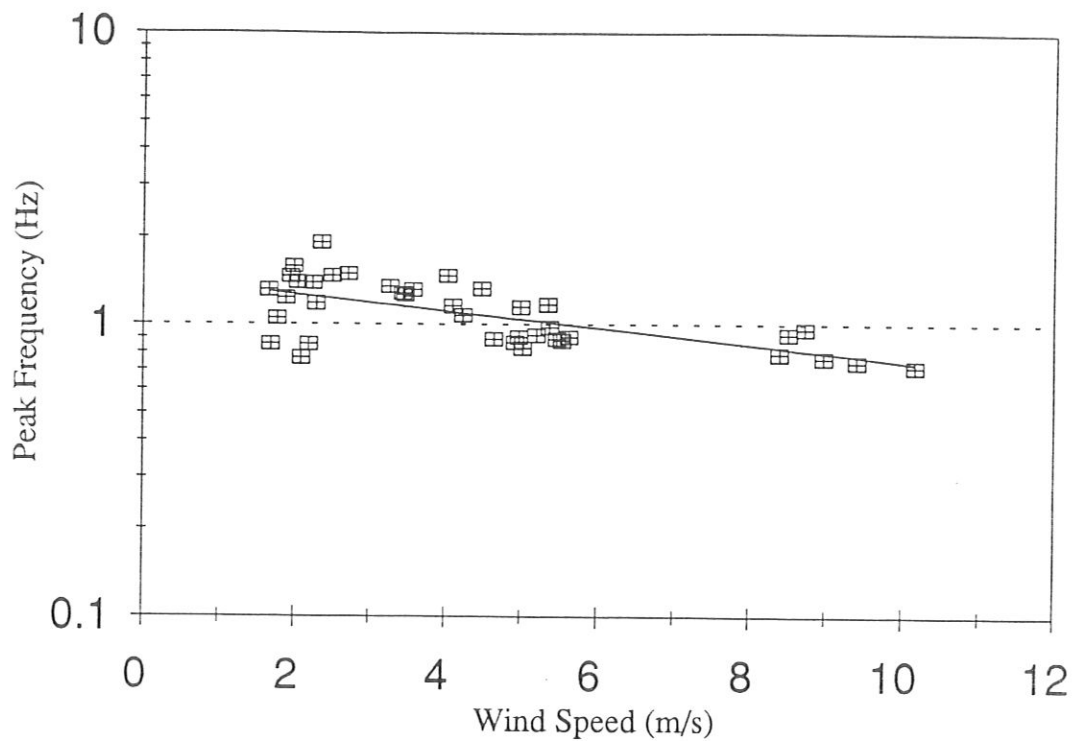


Figure 3.9 Scatter plot of wind speed vs. peak frequency.

these data sets displayed a variety of wind speeds from approximately 0 to 15 m/s. These plots show that there is a strong correlation between the wind speed and the dominant frequency of the power spectrum.

The second study of the wind data also shows a variation with wind speed. As the wind speed increases, the surface of the water becomes roughened. (Fig. 3.10) This roughening of the water changes the variance of the measured data set. Unlike the dominant frequency, change in variance of the data set is directly (as opposed to inversely) proportional to wind speed. Again, different deployments are used to illustrate the wind dependence on the variance of the data set. Figure 3.11 shows that there is indeed a strong correlation between wind speed and the variance of the data set. The parameters for the linear fit are $a_0 = 0.370$ and $a_1 = -0.166$.

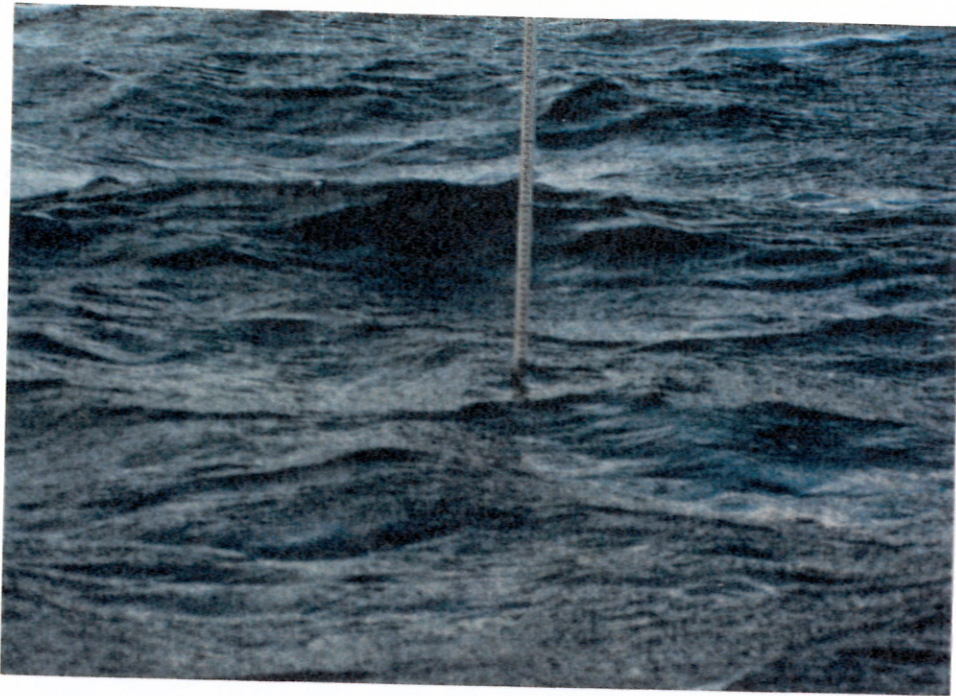


Figure 3.10a

Wind Speed (m/s)

Figure 3.11 Scatter plot of variance vs. wind speed.

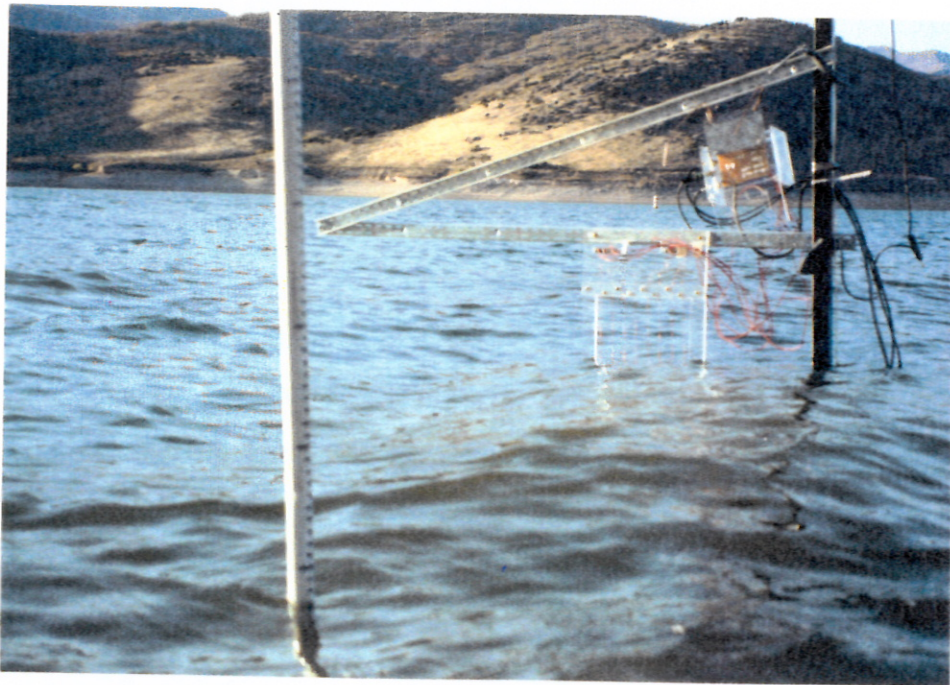


Figure 3.10b Comparison of surface roughness for high wind speeds (a) and low wind speeds (b).

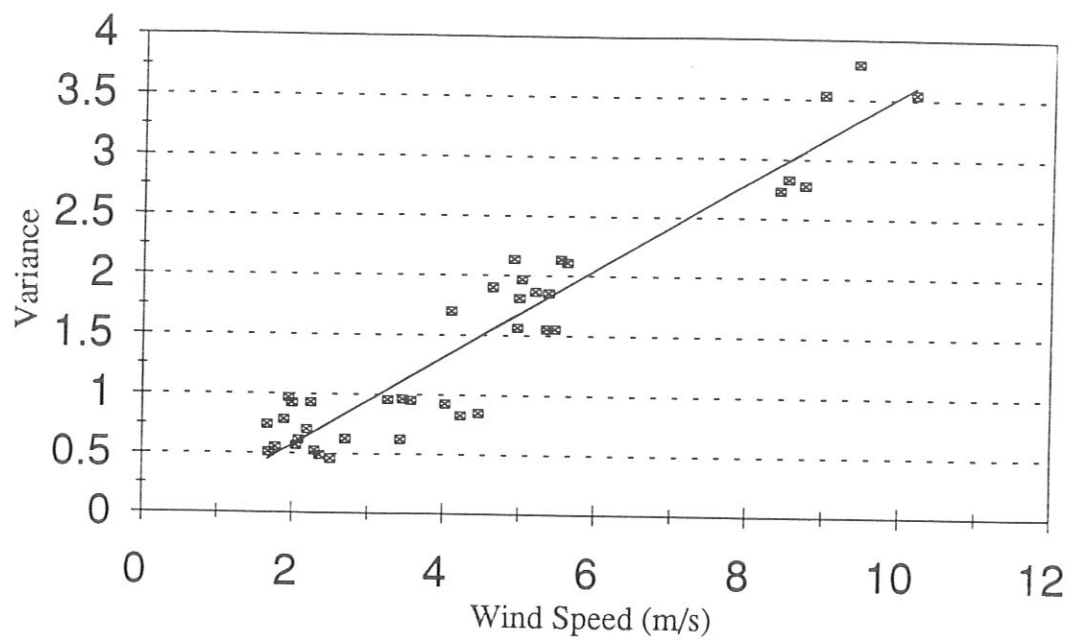


Figure 3.11 Scatter plot of variance vs. wind speed.

CHAPTER 4

CONCLUSIONS

4.1 Discussion

A wire wave gauge array that measures water wave displacement by means of capacitance wires has been successfully developed. This instrument will be used to gather data that will augment current scatterometry research at Brigham Young University.

Two different arrays were constructed. The first (referred to as the one-dimensional "harp" array) was used for laboratory testing and initial analysis of the capacitance wires as a means of acquiring water wave data. The second (referred to as the two-dimensional array) was built to increase the flexibility of the array and to provide data from two orthogonal directions simultaneously. Both arrays proved useful in providing the type of data they were designed to gather.

The accuracy and precision of the wave gauge were defined and studied to quantify the performance of the instrument. Laboratory tests showed a slow drift in the accuracy that was traced to temperature dependent gain variations of an amplifier. This drift in accuracy didn't effect the analysis because the slowly varying mean, which would represent a tidal action, is not of interest and was removed from the data at regular intervals. The precision of the instrument was found to have an average on the order of .1 mm. The initial goal was to measure waves with 1 mm amplitude. Data from the field deployments showed that the array could detect waves that ranged from roughly .03 to 6 m. The lower frequencies that were listed in the introduction are not present in lakes, but the array should be able to detect them as well.

Data gathered from field deployments demonstrated that the instrument was in fact sensing wind generated waves. This conclusion came from tests on power spectra, dominant frequency vs wind speed, and roughness vs wind speed. For wind generated

waves, the power spectra, when plotted in log-log space, rolls off with a slope of $-5 \text{ dB}(\text{m}^2/\text{Hz})/\text{decade}$ [10]. Data from our field deployments displayed this same characteristic. The dominant frequency of the power spectrum was plotted against the wind speed in scatterplot form. The plot showed the relation between the dominant frequency and the wind speed to be inversely proportional. When plotted in log-linear space, the roll-off is a straight line. The final test showed the correlation between the roughness of the water (which is the variance of a data set) and wind speed to be directly proportional.

4.2 Future Work

This research has resulted in a prototype wave gauge system and has demonstrated the feasibility of the concept. Future improvements to the system include packaging the system together on one platform, optimizing the mean squared error algorithm, and incorporating other analysis of the data which will exploit the properties of the array. Making these modifications will move the system from experimental to functional.

Other work involves implementing different electronic hardware and changing the operating system to a single board computer. The change involves the incorporation of a rms converter chip in the electronic hardware. This would eliminate the need for the software to calculate rms values for the capacitor voltage. The computer would then only have to sample each of the rms voltages and store them in an array for further processing. This change alone would significantly decrease the amount of time required for data acquisition and allow for higher sampling of the wave field.

The change to the single board computer could be readily made if the rms converters were incorporated into the hardware design. This is because the computational requirements would be decreased so that a 286 could handle all of the operations. If this change were made, the long transmission lines and the amplifier that drifts with temperature would be eliminated from the hardware and replaced with a communication link to another computer on the shore.

REFERENCES

- [1] D. Arnold, *Electromagnetic Bias in Radar Altimetry at Microwave Frequencies*, PhD Thesis, Massachusetts Institute of Technology, 1992.
- [2] K. B. Katsaros, and S. S. Ataktuerk, "Relationship Between Wind, Waves and Radar Backscatter", *National Aeronautics and Space Administration Report No.: NAS 1.26:190912; NASA-CR-190912*, Washington DC, 30 Nov 91.
- [3] P. M. Smith, and G. D. McCardle, "Spar Buoy Design for the Measurement of Centimeter-Scale Surface Waves in the Deep Ocean", *Proceedings of Oceans 1990*, pp 158-163, 24-26 Sep 1990.
- [4] P. M. Smith, and C. S. Lin, "Laser Slope Guage and a Spar Buoy Wave Guage: Tools for the Validation of Microwave Remote Sensors", *Naval Ocean Research and Development Activity Report No.: NORDA-TN-301*, NSTL Station, MS, Dec 1984.
- [5] W. H. Hayt Jr., *Engineering Electromagnetics*, New York, NY, McGraw-Hill 1989.
- [6] G. L. Bradley, *A Primer of Linear Algebra*, Englewood Cliffs, NJ, Prentice-Hall, 1975.
- [7] P. V. O'Neil, *Advanced Engineering Mathematics*, Belmont California, Wadsworth Publishing Company, 1983.
- [8] J. D. Kraus, *Antennas*, New York, NY, McGraw-Hill, second edition, 1988.
- [9] A. V. Oppenheim, and R. W. Schaffer, *Discrete-time Signal Processing*, Englewood Cliffs, NJ, Prentice-Hall, 1989.
- [10] O. M. Phillips, *The Dynamics of the Upper Ocean*, Cambridge, UK, Cambridge University Press, Cambridge, 1977.

DEVELOPMENT OF A WIRE WAVE GAUGE ARRAY FOR MEASURING
WIND-GENERATED WATER WAVES

Charles W. Hedelius

Department of Electrical and Computer Engineering

M. S. Degree, March 1993

ABSTRACT

A wire wave gauge array which uses capacitance wires to record wave height as a function of time has been developed to assist current scatterometry research. When an enamel-coated wire is immersed into water, a capacitance is formed between the wire and the water. The value of the capacitance is proportional to the length of the submerged wire. This wire capacitance is then incorporated into an electronic circuit. The voltage across the wire capacitor is digitized and the magnitude is computed using a mean squared error algorithm. From the voltage magnitude, the wave height is inferred. The sensed voltage is maximized by placing a fixed capacitor in parallel with the wire capacitor. Two different mechanical arrays were constructed. The first was a small harp geometry with all of the wires located in the same plane. The second was much larger and all of the wires were located in two orthogonal planes. The performance of the array was determined in terms of precision (how tightly clustered a group of data from identical water conditions is) and accuracy (how far from the true value the calculated value is). From these parameters, it was determined that the array had a precision on the order of .1 mm and an accuracy on the order of .25 cm. Four different field deployments were planned and conducted at two different locations. Data gathered from these deployments were analyzed to evaluate the content with respect to wind speed. The data showed a linear relationship between wind speed and surface roughness, and an inversely proportional relationship between wind speed and the dominant frequency of the wind waves. The power spectra of the data displayed the same characteristics as the known wind-wave spectra.

COMMITTEE APPROVAL:



David G. Long, Committee Chair



David V. Arnold, Committee Member



Richard H. Selfridge, Graduate Coordinator